Cardiac neurotrophic signaling impairment, amyloid β, and the Alzheimer's disease heart

Andrea Elia[1], Rebecca Parodi-Rullan[1], Rafael Vazquez-Torres[1], Ashley Carey[1], Sabzali Javadov[2†], and Silvia Fossati[1].

[1]Alzheimer's Center at Temple (ACT), Department of Neural Sciences, Lewis Katz School of Medicine, Temple University, 3500 N Broad St, Philadelphia, PA 19140.

[2] Department of Physiology, University of Puerto Rico School of Medicine, San Juan, PR 00936-5067, USA

† Deceased.

Corresponding author: Silvia Fossati; silvia.fossati@temple.edu

Abstract

While a link between cardiovascular risk factors and increased Alzheimer's disease (AD) risk has been reported, it remains unclear whether AD pathology has a direct effect on cardiac function and myocardial innervation. AD and amyloidosis are known to impair neuronal function and affect brain neurotrophic factors (NGF and BDNF) expression. Amyloid aggregates and neuro-signaling impairments may also expose AD patients to peripheral nervous system deficits, promoting cardiac disorders. Here, we characterize cardiac physiology, amyloid pathology, neurotrophic factors loss, and the impoverishment of cardiac neuronal fibers in Tg2576-AD mice hearts, human cardiomyocytes in culture, and human AD post-mortem left ventricular (LV) heart tissue. We reveal that Tg2576 animals exhibit increased myocardial fibrosis, amyloid β (Aβ) deposition, and brain/heart-axis neurotrophic deficiencies, resulting in myocardial denervation and cardiac dysfunction. Aβ oligomers reduce BDNF expression in both human immortalized and iPSC-derived cardiomyocytes, by disrupting TrkB/CREB signaling. Analysis of human LV AD post-mortem tissue confirmed cell and animal results. Our findings elucidate a previously unknown mechanism of Aβ-induced cardiac neurotrophic signaling dysregulation, underscoring the relevance of heart degeneration in AD.

Keywords: Amyloid-β (Aβ); Alzheimer's disease; cardiac dysfunction; neuro-signaling pathway; iPSC-derived cardiomyocytes; human post-mortem heart; brain-heart axis

Translational Perspective

This research identified cardiac amyloid pathology, neurotrophic factor depletion, and reduced myocardial nerve function in a transgenic model of cerebral amyloidosis (Tg2576) and in human AD heart tissue. These findings carry significant diagnostic and therapeutic implications, emphasizing the role of neuro-signaling disruption in cardiac physiology impairment linked to AD. Our study advocates for considering cardiac complications in AD management and paves the way for future precision medicine approaches to enhance systemic clinical strategies for treating AD, proposing the cardiac neurotrophic signaling pathway as a potential therapeutic target.

1. Introduction

Alzheimer's disease (AD) is an escalating global health concern, anticipated to triplicate in prevalence by 2050, primarily due to population aging[1] . This complex neurodegenerative disorder is characterized by the progressive accumulation of insoluble amyloid-β (Aβ) plaques in the brain parenchyma together with neurofibrillary tangles formed by hyperphosphorylated tau. Besides Aβ plaques and tau buildups, about 90% of AD patients also show Aβ deposits in and around the cerebral vasculature, known as cerebral amyloid angiopathy (CAA). CAA contributes significantly to the progression of AD pathology by promoting neuroinflammation, neurovascular dysfunction, decreased brain clearance, increased blood-brain barrier (BBB) permeability, and eventually neurodegeneration[2, 3].

Despite the main symptoms of the disease predominantly concerning the central nervous system (CNS), emerging evidence highlights extracerebral implications of AD, involving peripheral organs such as the heart[4]. Although abundant attention has been given to the impact of cardiovascular risk factors on AD risk and progression[5-7], only recent studies suggest a direct effect of AD pathology on cardiac dysfunction, and reveal Aβ peptides (Aβ40 and Aβ42) and big tau accumulation in the cardiac tissue of AD patients[8, 9].

The accumulation of Aβ in the AD brain is known to significantly affect the expression of the two main neurotrophic factors, nerve growth factor (NGF) and brain-derived neurotrophic factor (BDNF) [10]. This neurosignaling pathway's maladaptive remodeling is associated with cognitive decline[11]. The production of neurotrophins such as BDNF is also important for peripheral organs and cells, including endothelial cells, muscle cells, and cardiomyocytes. BDNF operates through tropomyosin receptor kinase B (TrkB) stimulation, contributing to the activation of neuronal pro-survival genes, including BDNF itself, through cAMP response element-binding protein (CREB) signaling[12]. Additionally, BDNF exerts pleiotropic effects in endothelial cells, muscle cells, and cardiomyocytes. BDNF/TrkB/CREB signaling is crucial for proper heart development and function in adulthood[13]. It is plausible to hypothesize that the cerebral neurotrophic signaling degeneration in AD may be accompanied by a gradual decline also in peripheral levels and function of these neuromodulators. A lack of neurotrophic support may result in a severe derangement of the cardiac nervous system, potentially culminating in severe heart dysfunction.

Notably, declining circulating BDNF levels have also been linked to cardiac disease progression, particularly of ischemic origin[14].
However, the effects of AD pathology on the heart pathophysiology remain poorly understood, and whether and through what mechanisms AD and amyloidosis modulate NTFs levels and innervation in the cardiac tissue has not been previously explored. Also, whether specific Aβ aggregates such as toxic oligomers, which may accumulate in the AD heart, fuel cardiac neuro-signaling dysregulation, is still to be defined.

To address these questions, we analyzed whether and how the accumulation of cardiac Aβ aggregates affected peripheral innervation and NTFs expression in the heart of Tg2576 transgenic mice, one of the most widely used models of cerebral amyloidosis. We observed a progressive decline in cardiac function, that became significant in 13 months-old Tg mice compared to controls, and was accompanied by Aβ deposition, fibrosis, increase in cardiac mass and reduced contractility. We found a significant reduction in cardiac nerve fiber density and neurotrophins levels, adrenergic and neuronal fibers regeneration markers, in Tg2576 mice compared to controls. Through *in vitro* experiments on human AC16 cardiomyocytes, neuroblastoma cells, and validation in human-induced pluripotent Stem Cell-derived cardiomyocytes (hiPSC-CMs), we showed that exposure to Aβ oligomers significantly reduced the expression of BDNF in both neural and cardiac cells. BDNF acts through tropomyosin receptor kinase B (TrkB) stimulation, contributing to the activation of pro-survival genes, including BDNF itself, through cAMP response element-binding protein (CREB) signaling. We demonstrated that CREB levels were reduced in cardiomyocytes exposed to Aβ oligomers, and that a TrkB agonist could mitigate caspase 3 activation and apoptosis in Aβ-exposed cardiomyocytes. Finally, we validated these findings by analyzing the neurotrophic cardiac profile in human left ventricle (LV) post-mortem tissue from AD patients with CAA compared to age-matched heathy subjects, thus opening novel avenues for future investigations into the impact of AD pathology on cardiac physiology.
This study demonstrates that pathological Aβ oligomers induce cardiac neuro-signaling impairment in mouse models and human AD hearts, elucidates the molecular mechanism responsible for Aβ-mediated cardiac neurotrophic deficiency and nerve fiber loss in AD, and may suggest novel therapeutic avenues to tackle this devastating

disease, contributing to filling an important gap on the effects of AD on cardiac function and pathology.

2. Methods

Animal Model

Male and female Tg2576 mice, a model of cerebral amyloidosis bearing the Swedish mutation (KM670/671NL), and age-matched wild-type (WT) littermates were bred in-house. Mice were maintained under controlled conditions (~22°C and in a 12-hour light-dark cycle, lights on 7 am to 7 pm) with unrestricted access to food and water. The generation of B6; SJL-Tg (APPSWE)2576Kha mice (Tg2576) on a B6; SJL Mixed Background was described in[15] . Tg2576 mice are known to develop numerous cerebral parenchymal amyloid-β plaques at 11-13 months and CAA at 10-11 months[16]. All experiments and animal protocols were performed according to procedures approved by the Institutional Animal Care and Use Committee of Temple University School of Medicine and conformed to the National Research Council Guide for the Care and Use of Laboratory Animals published by the US National Institutes of Health (2011, eighth edition).

Assessment of cardiac function by transthoracic echocardiography

Transthoracic bi-dimensional M-mode echocardiographic analysis was accomplished in 4, 8 and 13 months-old mice (before and after the development of brain Aβ pathology), under anesthesia, using a VisualSonics Vevo 2100 system (VisualSonics, Toronto, Canada). Before echocardiographic evaluation, the chest of the mice was carefully depilated by an operator. Subsequently, the mice were positioned in a clinostatic orientation on a temperature-controlled surface, with ECG leads embedded for monitoring, ensuring a constant temperature of 37°C. Anesthesia was then administered to the animals via an anesthetic chamber, utilizing isoflurane (Zoetis IsoFlo, Kalamazoo, MI), with an induction concentration of 3.0% and a maintenance range of 1–2.5%. This anesthesia regimen was meticulously managed to keep the animals within the desired anesthesia depth throughout the procedure, optimizing their physiological stability. Cardiac function and structure were evaluated by measuring left ventricle (LV) wall thickness, end-diastolic diameter (LVEDD), end-systolic diameter (LVESD), end-diastolic volume (LVEDV), end-systolic volume (LVESV), ejection fraction (EF%), and fraction shortening (FS%) percentage[17]. In accordance

141 with established protocols[18], speckle tracking-based strain echocardiography (STE)
142 was conducted using a parasternal long-axis B-mode loop captured through the
143 VisualSonics Vevo 2100 system (VisualSonics). High-speed imaging was ensured,
144 with all recordings comprising 300 frames at a rate exceeding 200 frames per second,
145 digitally stored as cine loops. Subsequently, the images obtained underwent
146 comprehensive analysis using Vevo Strain Software (Vevo LAB 1.7.1). LV endocardial
147 strain was computed in both radial and longitudinal axes and expressed as peak strain
148 percentage. Additionally, LV deformation rate over time was evaluated and presented
149 as strain rate (SR; peak 1/s). Global and regional assessments of LV endocardial
150 longitudinal and radial strain, along with SR, were performed based on the average
151 measurements derived from six LV segments (comprising basal, mid, and apical
152 anterior segments, as well as basal, mid, and apical posterior segments). Regional LV
153 endocardial longitudinal and radial strain, along with SR, were analyzed individually
154 for each LV segment and then averaged across both the anterior and posterior walls.
155 Vector diagrams illustrating the direction and magnitude of endocardial deformation
156 were acquired from parasternal long-axis B-mode images and subjected to detailed
157 analysis. Diastolic dysfunction was assessed by utilizing the reverse peak option to
158 evaluate reverse global longitudinal strain (GLS) and global radial strain (GRS) rates,
159 which were derived from long-axis B-mode traces[18, 19]. Lastly, animals were
160 euthanized at 13 months for organ explant and biomolecular and histological analysis.

161 **Tissue processing and morphological evaluations**

162 Cardiac specimens were fixed in Zamboni's solution (2% paraformaldehyde and picric
163 acid) overnight at 4°C, then cryoprotected with 20% sucrose in PBS for 24 hours at
164 4°C and cut in 5-μm-consecutive thick longitudinal sections using a cryotome (Leica
165 2000R, Germany). Interstitial fibrosis was assessed via Picrosirius Red Stain Kit
166 (Abcam, ab150681), and images were acquired using a Nikon NiE Fluorescence
167 Microscope with an 20X objective[20]. Cardiac fibrosis density was measured using
168 ImageJ software (NIH, version 1.30) and expressed as a percentage of fibrotic area
169 over the total area. A single operator blindly executed all the quantifications.

170 **Immunostaining**

171 The cardiac sections were processed via the indirect immunofluorescence method
172 using rabbit polyclonal antibodies against tyrosine hydroxylase (TH, Millipore, AB152;

173 1:100) to stain adrenergic nerve fibers and growth association protein 43 (GAP-43,
174 Millipore, #AB5220; 1:100) for regenerating nerve terminals. Cardiac nerve fibers
175 showed a regular pattern along cardiomyocytes[21]. Heart nerve ending density was
176 quantified using a square grid with 24 probes (area: 1 cm^2 each) overlapped to the
177 digital images, which were acquired using a Nikon Eclipse Ti fluorescence microscope
178 with 20X and 60X objectives. Five areas were randomly chosen for quantification from
179 each sample's three sections. The total number of intercepts between nerve fibers and
180 probes for each area was assessed, and cardiac nerve fiber density was measured
181 and expressed as the mean number of intercepts per area (fibers/mm^2). A single
182 operator assessed all the measurements blindly. Next, to evaluate amyloid-β
183 accumulation, 5- μm-thick cardiac sections from each experimental group were
184 marked with 6E10 anti-Aβ antibody (Covance, SIG-39320; 1:500) and co-stained with
185 cardiac troponin T (cTnT, Thermo Scientific, #MA5-12960; 1:250), collagen type I
186 (Rockland Immunochemicals, #600-401-103-0.1; 1:100), cardiac Troponin I (cTnI,
187 Abcam, ab47003; 1:200), or cleaved caspase-3 (Asp175) (Cl-Casp-3, Cell Signaling,
188 #94530; 1:200) antibodies. Additionally, to characterize βsheet (fibrillar) amyloid
189 deposits, cardiac sections were stained with Thioflavin-S solution (Acros organics,
190 213150250; 0.5g of Thioflavin-S powder in 100 ml dH_2O) for 30 minutes at room
191 temperature shielding from the light. Next, the sections were dehydrated in 80%
192 ethanol and thus washed in PBS 1X buffer. Nuclei were labeled with 4', 6-diamidino-
193 2-phenylindole (DAPI, Sigma Aldrich, D9542; 1:5000), and sections were mounted
194 using an aqueous mounting medium. Digital images were captured and analyzed by
195 a Nikon Eclipse Ti fluorescence microscope with a 60X objective. To evaluate vascular
196 components, after fixation, cardiac specimens were cut into 5-μm-thick longitudinal
197 sections using a cryotome (Leica 2000R, Germany). Next, tissue sections were
198 incubated for 30' minutes at 4°C in a blocking solution (10% donkey serum
199 supplemented with 0.3% Triton X-100 in phosphate-buffered saline). Via indirect
200 immunofluorescence procedure, sections were analyzed using goat polyclonal
201 antibodies against CD31 (R&D Systems, AF3628-; 1:30) and α-smooth muscle actin
202 (α-SMA, Abcam, ab32575; 1:500) at 4°C overnight, followed by specific secondary
203 antibodies conjugated with cyanine 3 or cyanin 5 respectively, to stain vascular
204 network. For serum amyloid A3 immunostaining (SAA3), fixed 5-μm-thick cardiac
205 sections were retrieved with formic acid 70% solution (Thermo Scientific, #270480010)
206 for twenty minutes at room temperature, they were then stained using mouse

207 monoclonal antibody against SAA (Abbexa, abx018140, 1:50) for two hours at 37°C,
208 followed by specific secondary antibodies combined with Alexa Fluor 488-conjugated
209 anti-mouse IgG. DAPI was used to counterstain nuclei and cardiac sections were
210 mounted with a Vectashield vibrance antifade mounting medium (H-1000). To assess
211 the changes in the cross-sectional area (CSA) of cardiomyocytes, 5μm-thick cardiac
212 sections from each experimental group were incubated for 30 minutes at 4°C in a
213 blocking solution (10% donkey serum) and permeabilized with 0.3% Triton X-100 in
214 phosphate-buffered saline. The tissue sections were then stained with 5 μg/mL wheat
215 germ agglutinin (WGA, #W11261, Thermo Fisher Scientific, Waltham, MA, USA) as
216 previously described[22] (PMID: 34404991). Afterward, the sections were mounted
217 with Vectashield Vibrance antifade mounting medium (#H-1000). Digital images were
218 captured and analyzed using a Nikon Eclipse Ti fluorescence microscope with a 20X
219 objective. Five to six randomly selected fields per sample were analyzed, totaling 50-
220 60 cardiomyocytes per section (10 cells per area). The mean cardiomyocyte diameter
221 (μm) was measured using the ImageJ software. Lastly, to assess amyloid-β deposits
222 in the human heart, 5- μm-thick LV sections from healthy donors and AD with CAA
223 patients were stained with 6E10 anti-Aβ antibody (Covance, SIG-39320; 1:500) and
224 co-stained with cardiac Troponin I (cTnI, Abcam, ab47003; 1:200). Images were
225 acquired and examined using a Nikon Eclipse Ti fluorescence microscope with 20X
226 and 60X objectives. A single operator blindly performed all the procedures.

227 **Preparation of cell and tissue lysates and immunoblotting analysis**

228 Cellular and cardiac samples were homogenized using RIPA cell lysis buffer (Thermo
229 Scientific) enriched with phosphatases and protease inhibitors (Thermo Scientific).
230 Then, the lysates underwent sonication and were centrifuged for 10 minutes at 4°C at
231 13,000 rpm to discard the insoluble debris. Next, total protein amounts were quantified
232 via a dye-binding Pierce BCA protein assay kit (Thermo Scientific) and detected using
233 a spectrophotometer reader (SpectraMax i3x Multi-mode Microplate Reader,
234 Molecular Devices) at a wavelength of 562 nm. Equal yields of protein (20-40 μg) were
235 separated through SDS-PAGE and identified by western blot (WB) analysis. Total
236 lysates were used to evaluate the protein levels of NGF (Alomone labs, AN-240;
237 1:1000), BDNF (Alomone labs, ANT-010; 1:1000), GAP-43 (Millipore, #AB552;
238 1:1000), Cleaved Caspase-3- Asp175 (Cl-Casp-3, Cell Signaling, #94530; 1:500),
239 dopamine β hydroxylase (DβH, Millipore, #AB1536; 1:1000), human Aβ [mouse

240 monoclonal anti-Aβ antibodies mixture composed of 4G8 epitope (residues Aβ18-22,
241 Covance, SIG-39320; 1:1000) and 6E10 epitope (residues Aβ3-8, Covance, SIG-
242 39220; 1:1000)], serum amyloid A3 (SAA3, Abcam, #ab231680; 1:500) CREB (Cell
243 Signaling, #9197; 1:1000), fibronectin (Abcam, #ab2413; 1:1000), matrix
244 metalloproteinases- 2 (MMP-2, Cell Signaling, #35814; 1:1000), Laminin A/C (Santa
245 Cruz Biotechnology, sc-376248; 1:500), Actin (Millipore, MAB1501; 1:1000) and
246 GAPDH (Santa Cruz Biotechnology, sc-32233,6C5; 1: 2000), the three latter of which
247 were used as loading controls. Protein bands were detected using Odyssey® CLx
248 Imaging System according to the manufacturer's instructions and quantified with
249 Image Studio™ Lite Software[23].

250 **ELISA**

251 Aβ40 and Aβ42 peptide levels were detected using a commercial ELISA kit (Invitrogen
252 KHB3481 and KHB3441, respectively). Briefly, cardiac specimens for each mouse
253 were collected at the end of the experimental study and homogenized with RIPA cell
254 lysis buffer (Thermo Scientific), supplemented with phosphatases and protease
255 inhibitors (Thermo Scientific, Waltham, MA). Then, ELISA was performed using an
256 equal amount of total cardiac protein following the company's specifications, and the
257 plate was evaluated at 450 nm with a spectrophotometer reader (SpectraMax i3x
258 Multi-mode Microplate Reader, Molecular Devices).

259 **Aβ peptides**

260 Pre-aggregated Aβ40 and Aβ42 oligomers were generated from HFIP-pretreated and
261 lyophilized peptides as previously described[24]. Briefly, oligomer enriched Aβ40 and
262 Aβ42 preparations were obtained after a dilution of the lyophilized peptide in DMSO
263 at a concentration of 5 mM, then diluted to 100 μM in ice-cold DMEM/F12 media and
264 incubated at 4°C for 16 hours. Next, Aβ40 and Aβ42 oligomers were resuspended in
265 DMEM/F12 medium to 10 μM as a final concentration for the cell treatments.

266 **Cell culture and treatments**

267 Human ventricular myocardial cardiomyocytes (AC16, purchased from Millipore,
268 #SCC109) were expanded in 10 cm^2 dishes not further than the 10th passage, in a
269 humidified environment at 37°C with 5% CO_2 in DMEM/F12 medium (Lonza Ltd.
270 Basel, Switzerland) supplemented with 12.5% fetal bovine serum (FBS) and 1%

271 penicillin-streptomycin (P/S, Lonza). AC16 cells were grown in the pre-contractile
272 developmental stage, thus allowing us to better track molecular events and cellular
273 responses[25, 26], without the complications and variability associated with isolated
274 adult cardiomyocyte cultures. Human SH-SY5Y neuroblastoma cells (ATCC, CRL-
275 2266, a neuronal cell line used widely in experimental neurological studies[27-29])
276 were grown in 10 cm^2 dishes within the 10th passage in a humidified environment at
277 37°C with 5% CO_2 in DMEM/F12 medium (Lonza Ltd. Basel, Switzerland)
278 supplemented with 10% fetal bovine serum (FBS) and 1% penicillin-streptomycin (P/S,
279 Lonza). For both cell types, AC16 and SH-SY5Y, an equal number of cells were
280 seeded in 6 well plates, and after 24 hours, once they reached about 70- 80%
281 confluency, cells were challenged with human Aβ40 or Aβ42 oligomers (10 μM) for 16
282 hours. In certain studies, cells were treated with human Aβ40 oligomers (10 μM) for
283 either 15 minutes or 1 hour. For other experiments, cells were exposed to the
284 BDNF/TrkB receptor agonist LM22A-4 (100 nM) or the antagonist ANA-12 (30 μM) for
285 16 hours. LM22A-4 (4607) and ANA-12 (SML0209) were sourced from Tocris
286 Bioscience and Sigma Aldrich, respectively.

287 **Maintenance and treatment of Human-Induced Pluripotent Stem Cell-Derived**
288 **Cardiomyocytes (hiPSC-CMs)**

289 A commercially available hiPSC-CM line, iCell Cardiomyocytes[2] (Catalog number
290 R1220, Kit/lot 12,012; FUJIFILM Irvine Scientific, Inc., United States), was utilized for
291 this study. The cells were seeded into a 0.1% gelatin-coated 12-well plate at a density
292 optimized to form a monolayer (≈210K cells per well) and cultured in a stage incubator
293 (37°C, 5% CO2) following the provider's guidelines. Experiments were conducted 5–
294 7 days post-plating, ensuring the cells formed a viable, beating monolayer, in
295 accordance with the manufacturer's instructions (Supplementary Video). Cells from
296 this specific lot were from the same donor (healthy, female, Caucasian, age <18), as
297 verified by FUJIFILM Cellular Dynamics. For the experiment, hiPSC-CMs were treated
298 with human Aβ40 oligomers (10 μM) for 20 hours, after which the cells were collected
299 for biochemical analysis. For imaging, cells were fixed with 4% paraformaldehyde
300 (PFA) for 10 minutes, washed with 1X PBS, and then blocked and permeabilized for
301 30 minutes using PBS containing 0.1% Triton X-100 and 2% normal donkey serum.
302 hiPSC-CMs were subsequently labeled with a BDNF antibody (Abcam, ab226843;
303 1:250) and co-stained for cardiac troponin T (cTnT, Thermo Scientific, #MA5-12960;

304 1:250), with nuclei labeled using DAPI (Sigma Aldrich, D9542; 1:5000). Imaging was
305 conducted using a Nikon Eclipse Ti fluorescence microscope with a 100X objective,
306 with all procedures performed by a single operator in a blinded manner.
307
308 **Nuclear protein isolation**
309 AC16 human cardiomyocytes were cultured in 6 well plates until they reached
310 confluence and treated with human Aβ40 oligomers for 15 minutes. To extract the
311 nuclear fractions, cells were collected using buffer A, containing 10 mmol/L HEPES at
312 pH 7.9, 10mmol/L KCl, 0.1mmol/L EDTA, integrated with 25% NP-40X-100 non-ionic
313 surfactant detergent solution, enriched with protease inhibitors. The cell lysate was
314 transferred in a 1.5 ml tube, placed in ice, and centrifuged for 10 min at 4°C at 13,000
315 rpm to discard the insoluble debris. The supernatant was transferred to a new 1.5 ml
316 tube to preserve the cytosolic fraction, while the pellet was resuspended in fresh
317 prepared buffer B composed of 20mmol/L HEPES at pH 7.9; 0.4mol/L NaCl; 1mmol/L
318 EDTA; 10% glycerol; supplemented with protease inhibitor. Next, the tube containing
319 the nuclei pellet dissolved in buffer B was placed on a rotator for 2 hours at 4°C and
320 then centrifuged at 13,000 rpm for 5 minutes at 4°C. Lastly, the supernatant (nuclear
321 fraction) was transferred to a new 1.5 ml tube and stored at -80°C, ready for the
322 following protein quantification and immunoblot analysis[23].
323
324 **Human LV specimens**
325 Frozen human LV post-mortem tissue from healthy donors and patients with clinical
326 diagnoses of AD and CAA were obtained from the Banner Sun Health Research
327 Institute clinical biobank to investigate the impact of AD pathology on myocardial
328 innervation. The selection criteria of the study population excluded individuals with
329 comorbidities known to substantially affect cardiac function, including high blood
330 pressure, cerebrovascular accidents (e.g., strokes and lacunes), brain/cardiac
331 neoplastic conditions, secondary amyloidosis, prior myocardial infarction, and
332 endocarditis. Healthy volunteers and AD+CAA patients were matched based on age,
333 sex, and ethnicity. Human cardiac specimens were used for biochemical and
334 histological characterization.
335
336
337

338 **Statistical methods and analysis**

339 Data are expressed as means±SEM. A two-tailed Student's t-test determined the
340 statistical significance between the two groups. When comparing multiple groups, data
341 were analyzed using a one-way or two-away analysis of variance (ANOVA) test,
342 followed by Tukey's post hoc test. Outliers were identified and excluded from the
343 original dataset using the ROUT (Q = 1%) method with GraphPad Prism 9.1.0
344 software. Differences between groups were considered statistically significant when
345 $p \leq 0.05$. All data were analyzed and graphically represented using GraphPad Prism
346 software version 9 (GraphPad, La Jolla, CA).

347 **3. Results**

348 **3.1. AD pathology promotes cardiac dysfunction, Aβ accumulation, and**
349 **misfolding of serum amyloid A3 in the heart of Tg2576 mice.**

350 To assess the impact of AD amyloid pathology on cardiac tissue physiology and
351 systolic activity, we conducted echocardiographic analyses in Tg2576 transgenic
352 mice, and age-matched WT littermates, both before and after the development of
353 cerebral Aβ pathology (at 4 and 8, or 13 months, respectively). Bi-dimensional M-mode
354 tracings revealed a significant decrease in left ventricular ejection fraction (EF%) and
355 fractional shortening (FS%) percentage in 13-month-old Tg2576 mice compared to
356 WT animals (Fig. 1A-B, and other cardiac echocardiographic parameters in
357 Supplementary Table 1). Radial and longitudinal strain/strain rates were also analyzed
358 in both animal groups. Tg2576 exhibited global (average of 6 LV segments) and
359 anterior-apical longitudinal strain impairment compared to WT mice, with severe
360 longitudinal contractility dysfunction that affects the anterior-basal segment
361 (Supplementary Fig. 2). Younger Tg2576 cohorts (at 4 or 8 months) did not exhibit
362 significant changes in cardiac physiology (Supplementary Fig. 3), despite the
363 presence of Aβ deposits in the brain starting at 8 months (Supplementary Fig. 5).
364 Furthermore, 13-month-old transgenic mice displayed notable left ventricle
365 enlargement, evidenced by increased left ventricular end-systolic diameter, leading to
366 elevated left ventricular end-systolic volume (LVESV, Supplementary Table 1). The
367 gravimetric analysis confirmed a significant increase in the heart weight/body weight
368 ratio in 13-month-old Tg2576 mice compared to the WT group (Fig. 1C), further
369 corroborated by the increased cardiomyocyte cross-sectional area assessed through

370 WGA staining (Supplementary Fig. 1). Cardiac dysfunction in the Tg2576 mice
371 coincided with a marked increase in myocardial interstitial fibrosis, as evidenced by
372 Picrosirius red staining (Fig. 1D-E), accompanied by amyloid β accumulation in
373 Tg2576 myocardial parenchyma (Fig. 1L) that contributes to a cardiac stiffness
374 enhancement. Immunostaining results were confirmed via WB analysis, which shows
375 high levels of fibronectin, a key component of the extracellular matrix (ECM) [30], in
376 the Tg2576-AD mouse heart (Supplementary Fig. 1). However, in line with another
377 recent AD study [31], no significant changes in cardiac MMP-2 levels between the WT
378 and transgenic AD mice were observed (Supplementary Fig. 1).
379 Using peptide-specific ELISA assays, we confirmed a significant increase in Aβ40
380 levels in 13-month-old Tg2576 cardiac tissue compared to WT mice, while no
381 substantial changes in Aβ42 levels were noted between the two groups (Fig. 1F-G).
382 These findings align with the age dependent Aβ pathology in the Tg2576 mouse
383 model, characterized by higher abundance and progressive increase in cerebral Aβ40
384 levels compared to Aβ42[32]. Western blot analysis further validated the cardiac Aβ40
385 deposition detected by ELISA, confirming a significant increase in Aβ dimers and
386 oligomers in total heart lysates of 13 months old Tg2576 mice compared to WT
387 littermates (Fig. 1H-I-J). Immunofluorescence staining revealed amyloid aggregates
388 accumulating in interstitial spaces between cardiomyocytes, alongside collagen fibers,
389 corroborating the myocardial interstitial fibrosis observed via Picrosirius red staining
390 (Fig. 1L, top panels, and Supplementary Fig. 6B). Besides Aβ aggregates, reports
391 have demonstrated amyloid precursor protein (APP) expression in peripheral organs,
392 including the myocardium, suggesting the potential production of Aβ outside the brain
393 parenchyma[9, 33, 34]. Consistent with this, but also with the fact that the prion protein
394 promoter may be expressed in other innervated tissue, including in the heart, we
395 observed APP upregulation in the plasma and cardiac tissue of Tg2576 mice
396 (Supplementary Fig. 8). Aβ challenge has been linked to increased apoptosis in
397 various cell types, including cardiac cells, and in AD brains[35, 36]. Indeed, analysis
398 of cardiac tissue by western blotting and immunohistochemistry revealed elevated
399 levels of cleaved-caspase 3 in Tg2576 cardiomyocytes (Fig. 1K, 1L bottom panels,
400 1M).
401 As AD pathology is characterized by progressive protein misfolding, seeding
402 processes may be initiated by different amyloids interacting with each other[37].
403 Therefore, the accumulation of misfolded Aβ oligomers in the heart tissue may

404 contribute to increased fibrosis and to the seeding of other amyloid peptides, such as
405 serum amyloid A (SAA) proteins. Although high levels of SAAs typically do not lead to
406 fibrillar deposits, chronic inflammatory states or seeding processes (e.g., promoted by
407 Aβ) may induce the accumulation of SAA peptides in peripheral tissues[38, 39].
408 Indeed, we observed Aβ aggregates around cardiac vessels in aged Tg2576 mice,
409 accompanied by infiltration of the vascular basal lamina (Supplementary Fig. 4,
410 Supplementary Fig. 6, *bottom panels*, and Supplementary Fig. 7D), alongside
411 increased serum amyloid A3 (SAA3) vascular deposits (Fig. 1N). Immunoblot analysis
412 confirmed increased SAA3 dimers in the cardiac tissue of Tg2576 mice (Fig. 1O-P).
413 Overall, these findings indicate that AD pathology detrimentally affects systolic
414 function and cardiac tissue structure. Progressive interstitial and perivascular Aβ
415 deposits contribute to cardiac cell apoptosis and aggregation of serum amyloid
416 proteins, culminating in cardiovascular dysfunction. Notably, 8-month-old Tg2576
417 mice exhibited evident amyloid aggregate accumulation in the prefrontal cortex
418 vasculature and cerebral parenchyma (Supplementary Fig. 5), consistent with
419 literature describing early Aβ deposition and CAA in the Tg2576 brain[32]. However,
420 no significant changes were observed in Aβ accumulation in the hearts of 8-months
421 old Tg2576 mice compared to the older transgenic cohort (Supplementary Fig. 5 and
422 Supplementary Fig. 6), confirming that Aβ pathology starts in the brain of these mice,
423 followed by a later increase in cardiac Aβ levels.

424 **3.2. Neurotrophic signaling is impaired in the heart of AD transgenic mice.**

425 AD pathology and Aβ deposition are known to profoundly disrupt neurotrophins
426 production in the brain, contributing to the progressive loss of key neuromodulators,
427 including NGF and BDNF, ultimately leading to cognitive decline and dementia[40,
428 41]. However, whether AD pathology can modulate peripheral neurotrophic activity
429 and cardiac innervation remained to be elucidated. Therefore, we explored the
430 regulation of neuro-signaling modulators and innervation factors in both cerebral
431 cortex and cardiac lysates of 13-month-old Tg2576 mice. Immunoblotting analysis
432 revealed a marked decrease in both cerebral and cardiac levels of NGF and BDNF
433 expression in the Tg2576 group compared to WT littermates (Fig. 2A-B). This
434 reduction in neurotrophins levels observed in transgenic mice was accompanied by a
435 significant decrease in the adrenergic marker (DβH) and the neuronal fibers
436 regeneration marker, GAP-43 (Fig. 2A-B). Intriguingly, immunohistochemistry analysis

437 corroborated a notable loss in cardiac nerve fiber density in Tg2576 mice compared
438 to WT animals, including reductions in sympathetic and regenerating nerve endings
439 labeled with TH and GAP-43 markers, respectively (Fig. 2C-D-E and Supplementary
440 Fig. 7A-C). These findings suggest that AD amyloid pathology may have detrimental
441 effects on peripheral neurotrophic pathways, thereby impacting the peripheral nervous
442 system and cardiac innervation.
443

444 **3.3. Aβ oligomers impair neurotrophins production in hiPSC-CMs, AC16**
445 **cardiomyocytes and neuroblastoma cells.**

446 Our *in vivo* investigations revealed a notable decrease in neurotrophic markers and
447 nerve fibers within the cardiac tissue of Tg2576 mice. To ascertain whether this loss
448 of NTFs can be caused by the Aβ aggregates present in the heart, we evaluated the
449 impact of Aβ40 oligomers, recognized as the most toxic amyloid aggregates and
450 preferentially enriched in the AD brain vasculature, on the production of neurotrophins
451 and neuronal regeneration markers in both human iPSC-CMs and AC16
452 cardiomyocytes (Fig. 3 and Fig. 4). Aβ40 oligomers significantly reduced BDNF
453 expression in hiPSC-CMs and AC16 cardiomyocytes (Fig. 3E-F and Fig. 4). In
454 addition, the effects of Aβ42 oligomers, the main toxic species coming in contact with
455 neurons in the brain parenchyma, were examined on neuronal SHSY-5Y cells.
456 Following a 16-hour incubation with Aβ oligomers, a significant reduction in protein
457 levels of GAP-43 and BDNF was observed in neuronal cells, with no substantial
458 changes in NGF expression (Fig. 3A-D). These findings support the hypothesis that
459 Aβ toxic aggregates contribute to the impairment of the cardiac neuro-signaling and
460 neural regeneration pathways by diminishing the production of BDNF in both neurons
461 and cardiomyocytes and reducing levels of GAP-43 in neurons.

462 **3.4. Neurotrophic factors are reduced in the heart of Alzheimer's disease**
463 **patients with cerebral amyloid angiopathy.**

464 To confirm the clinical and translational relevance of our findings in human AD, we
465 investigated the cardiac neurotrophic profile in LV biopsies obtained from patients
466 affected by AD along with CAA. Our study cohort comprised individuals clinically
467 diagnosed with AD, confirmed through anatomopathological examination, excluding
468 cases affected by other conditions that could significantly impair cardiac function, such
469 as high blood pressure, secondary amyloidosis, stroke, brain and cardiac neoplastic

470 conditions, prior myocardial infarction, and endocarditis. Healthy volunteers and
471 AD+CAA patients were matched based on age, sex, and ethnicity (Table 1). Our
472 analysis revealed significantly reduced levels of BDNF, downregulation of the
473 sympathetic marker tyrosine hydroxylase (TH), and a decline in GAP-43 protein
474 expression in the heart of AD+CAA subjects, confirming the deterioration of
475 neurotrophic factors and the neuro-signaling pathway in the human AD heart (Fig. 5A-
476 B), with enormous clinical implications. Immunostaining analysis showed amyloid-β
477 deposits in the myocardial parenchyma of human AD patients with CAA (Fig. 5C). In
478 aggregate, these findings demonstrate a myocardial neuro-signaling impairment
479 associated to Aβ deposition in human AD hearts, supporting our experimental *in vitro*
480 and *in vivo* results.

481 **3.5. Aβ40 oligomers impair BDNF/TrkB/CREB signaling in human**
482 **cardiomyocytes.**

483 The downregulation in BDNF expression observed in our *in vitro* and *in vivo*
484 experiments prompted us to investigate the mechanism by which Aβ affects the
485 cardiac BDNF pathway. BDNF/TrkB/CREB signaling impairment is involved in age-
486 related synaptic deterioration and neurodegenerative disorders, culminating in
487 cognitive decline and neuronal loss. Indeed, AD patients exhibit significant depletion
488 of BDNF expression in cerebrospinal fluid, post-mortem brain tissue, and
489 bloodstream[42]. The detrimental impact of Aβ oligomers on BDNF exon IV transcript
490 in neuronal cells is associated with decreased CREB levels, the critical mediator of
491 BDNF transcription[43, 44]. Consistent with these findings, here we observed a
492 significant reduction in nuclear CREB levels in human cardiomyocytes following
493 treatment with Aβ40 oligomers (Fig. 6A-C), suggesting that a reduction in CREB
494 transcriptional function mediates both the reduced levels of BDNF and the impact on
495 the other neurotrophic markers. These results confirm the critical role of the
496 BDNF/CREB axis in AD cardiac pathology, unveiling an Aβ-dependent signaling
497 mechanism which can explain the BDNF reduction we observed in AD. To confirm the
498 protective effect of TrkB activation in our model, we stimulated human cardiomyocytes
499 with the selective TrkB receptor agonist, LM22A-4[45] (Fig. 6D-E), in the presence or
500 absence of Aβ40 oligomers[46]. Remarkably, LM22A-4 stimulation reduced Aβ40-
501 mediated caspase 3 activation, thereby mitigating apoptosis, and confirming the
502 protective effects of BDNF signaling on cardiac cells (Fig. 6G-H). Conversely, ANA-

503 12, a specific BDNF/TrkB receptor antagonist[47] (Fig. 6D-F), exacerbated
504 cardiomyocyte caspase 3 activation, (Fig. 6G-I), Overall, these findings elucidate the
505 mechanisms and impact of the neurotrophic signaling deregulation induced by Aβ
506 pathology in the heart (Supplementary Fig. 9), highlighting the protective role of
507 BDNF/TrkB/CREB signaling in cardiomyocyte homeostasis.

508 **4. Discussion**

509 This study demonstrates that, similar to what was previously observed in the brain, Aβ
510 deposition in the AD heart leads to neurotrophic signaling impairment, which
511 contributes to increased cardiomyocyte apoptosis and severe cardiac morphological
512 and functional impairment observed in the hearts of Tg2576 mice. Confirming the
513 clinical validity of these findings, the neurotrophic changes and the presence of Aβ
514 pathology were validated in human post-mortem heart samples from patients with
515 AD+CAA. Our data suggest that cardiac amyloidosis (evidenced by the presence of
516 Aβ and SAA3 oligomers) contributes to interstitial fibrosis and to the loss of
517 neurotrophins, resulting in cardiac innervation deficits and neuro-signaling pathway
518 impairment, which appear to be essential mediators of the observed cardiac
519 physiological dysfunction. The heart-brain axis constitutes a complex and highly
520 regulated bi-directional interconnection between the central and peripheral nervous
521 systems.[48]. Neurodegenerative pathologies, such as AD, may have severe and
522 debilitating effects on various peripheral organs, including the heart, through the
523 modulation of both the central and peripheral nervous systems. However, the impact
524 of AD pathology and Aβ accumulation on cardiac neuro-signaling pathways in AD
525 patients and animal models has not been previously elucidated. An increasing number
526 of studies are beginning to highlight the involvement of cardiac tissue in
527 neurodegenerative diseases, revealing a compelling interplay between AD and
528 cardiac disorders[49], such as atrial fibrillation[50], heart failure[51], and coronary
529 artery disease[34]. It has recently been shown that AD patients exhibit myocardial
530 dysfunction following the deposition of Aβ aggregates in cardiac tissue [9], and the
531 presence of cardiac N-terminal cleavage products of APP was correlated with levels
532 of CAA and myocardial fibrosis[52]. In line with this, Sanna and coworkers described
533 the presence of structural and functional abnormalities in the cardiac tissue of a small
534 cohort of AD subjects[4].

535 AD pathology has been shown to severely impact the production and release of the
536 main NTFs, NGF and BDNF, in the brain[53, 54]. These two neurotrophins are mainly
537 involved in the maturation and differentiation of neurons, regulating neurogenesis and
538 synaptogenesis[55, 56]. The progressive decline in NTFs expression due to aging,
539 exacerbated by AD pathology, may lead to an adverse remodeling of the whole neuro-
540 signaling pathway, driving, together with other AD pathological factors such as amyloid
541 oligomers, an impairment of the peripheral innervation[41].
542 This study demonstrates the effect of Aβ pathology on cardiac physiology and heart
543 dysfunction using a transgenic mouse model of AD with CAA, human cardiomyocytes
544 in culture, validated also in hiPSC-CMs, and AD+CAA human post-mortem heart
545 tissue. It describes the mechanisms underlying the impairment of peripheral
546 innervation and the loss of neurotrophins in the AD heart and shows a causal role of
547 Aβ oligomers in the impairment of neurotrophic signaling in cardiomyocytes. We report
548 that Tg2576 mice show an age-dependent deterioration in cardiac function and a
549 gradual replacement of viable myocardial with fibrotic tissue, resulting in interstitial
550 fibrosis. This cardiac maladaptive remodeling, which develops after the brain Aβ
551 deposition, is accompanied by an increased cross-sectional area alongside a
552 significant accumulation of Aβ, particularly Aβ40, localized in cardiac perivascular and
553 interstitial spaces with collagen deposits. Caspase 3 activation within cardiomyocytes
554 is also increased, suggesting that Aβ aggregates in the heart tissue contribute to the
555 development of interstitial fibrosis and apoptotic cardiac cell death. The preferential
556 accumulation of Aβ40, rather than Aβ42, in Tg2576 mice hearts is in line with previous
557 studies describing the progressive increase mostly of Aβ40 levels in both serum and
558 brain parenchyma of Tg2576 mice during aging[32]. Additionally, the Aβ40 peptide is
559 preferentially associated with vascular deposits and CAA in the human brain, resulting
560 in degenerative phenotypes in cerebral endothelial cells [36], which culminate in
561 vessel wall dysfunction[35], contributing to BBB permeability and
562 microhemorrhages[57]. This increased BBB permeability in AD brains may enhance
563 the systemic diffusion of Aβ40 (including aggregated forms such as oligomers) through
564 the blood and its accumulation in peripheral organs, including the heart. Indeed, Aβ40
565 is the most abundant peptide in the cerebrospinal fluid and blood of AD patients, and
566 multiple biomarker studies have shown that this peptide does not decrease in
567 peripheral organs and tissues with AD progression[58]. Conversely, as Aβ42 fibrils

accumulate in the brain parenchyma, Aβ42 levels decrease in the cerebrospinal fluid and in the peripheral blood[59].

It is known that Aβ oligomers may act as “seeds”[60] to induce aggregation of other amyloids. Some of these aggregation species fuel cell stress and inflammation, resulting in degenerative processes in multiple cell types, including endothelial and cardiac cells, as our group and others have shown[61, 62]. Here, we show that SAA3 also accumulates in the heart of Tg2576 mice, likely contributing to amorphous and misfolded protein accumulation and to progressive cardiac impairment. SAA3 is involved in vascular injury as a promoter of atherosclerosis, and it is a prognostic factor for coronary artery syndromes, also proposed as a novel inflammatory marker for ischemic heart disorders[63-65]. Notably, we observed SAA3 aggregates accumulate primarily at the cardiac vessel walls, together with Aβ deposits, suggesting that misfolded Aβ peptides or oligomers may diffuse through the vascular system, reaching the heart, with consequential seeding of other systemic amyloids around the myocardial vessels. Interestingly, no changes in cardiac physiology and no evidence of amyloid deposits were found in younger (4 or 8 months) Tg2576 mice. However, Aβ deposits were already detected around brain vessels in the prefrontal cortex of 8-month-old Tg2576 mice. Thus, it is reasonable to think that, in this model and presumably in AD patients, cardiac dysfunction may be subsequent to the progressive accumulation of amyloid aggregates in the brain, particularly as CAA, in and around the brain vessels. Given the extensive scientific results, we sustain that the cardiac disease and maladaptive heart remodeling resulting from progressive amyloid deposition in the heart also contribute to cognitive decline, thereby exacerbating AD pathology in a destructive feed-forward loop.

Notably, we observed pro-apoptotic markers (active caspase 3) in cardiomyocytes exposed to Aβ oligomers in vitro and in vivo, suggesting a direct effect of Aβ pathological aggregates on the impairment of cardiac cell function. Interestingly, caspase 3 activation is also associated with tau cleavage at position 421, which promotes increased tau phosphorylation[66], suggesting possible downstream effects that may precipitate tau pathology, which was recently described in the heart by the Del Monte group[8, 67]. Notably, we revealed a depletion in both adrenergic nerve endings and regenerated nerve terminal fibers in the transgenic AD mouse hearts. This myocardial denervation was associated with a reduction of NGF and BDNF at both the cerebral and cardiac levels, accompanied by significant impairment in the

602 neuronal sprouting marker GAP-43. Importantly, post-mortem AD human hearts also
603 exhibited a reduction in BDNF expression, as well as in the cardiac nerve fiber markers
604 TH and GAP-43. In AD patients, the decline of neuromodulators in the brain is known
605 to accelerate age-related synaptic loss, resulting in cognitive impairment[68, 69]. NTFs
606 are powerful biomolecules with significant pleiotropic effects involved in cellular growth
607 and survival pathways in both the brain and peripheral cells/tissues, including
608 endothelial cells, muscle cells, and the cardiovascular system[22]. Our finding that
609 after treatment with Aβ oligomers, BDNF and GAP-43 expression in human neurons,
610 endothelial cells, and both hiPSC-CMs-derived and immortalized cardiomyocytes
611 were significantly reduced suggests a direct effect of Aβ in lowering NTFs not only in
612 neuronal cells, and possibly peripheral neurons, but also in endothelial cells and
613 cardiomyocytes. This reduction may cause AD patients to be more susceptible to
614 developing cardiovascular disorders of various etiologies[70, 71].
615
616 To validate the mechanism inducing this cardiac Aβ-mediated neuro-signaling
617 deterioration, we manipulated the BDNF signaling pathway pharmacologically in
618 human cardiomyocytes. Cells treated with LM22A-4, a competitive agonist of the
619 BDNF receptor TrkB, showed a reduction in Aβ40 oligomers-mediated caspase 3
620 activation, confirming a TrkB-dependent mechanism linking reduced BDNF to the Aβ-
621 mediated cardiomyocyte toxicity. LM22A-4 was also reported to alleviate cardiac
622 ischemia-induced apoptosis and to improve neuronal outgrowth and myocyte
623 physiology with endothelial cell proliferation, thus arresting chronic heart failure[14].
624 Moreover, LM22A-4 showed effects similar to BDNF in preventing Aβ-induced
625 neuronal cell death[45]. These beneficial effects suggest the initiation of a myocardial
626 autocrine/paracrine protective pathway through TrkB activation, which may include the
627 increased transcription of BDNF itself, via CREB activation[14].
628 In line with this concept, we demonstrated a significant downregulation of CREB
629 nuclear expression (necessary for its transcriptional function) in cardiomyocytes
630 challenged with Aβ40 oligomers. CREB is the leading transcription factor activated
631 upon BDNF-TrkB binding, which also promotes, in a feed-forward loop, the
632 transcription of BDNF itself. Our results provide a mechanistic explanation of how Aβ
633 oligomers can promote a CREB-mediated downregulation of BDNF expression in
634 cardiomyocytes, uncovering a previously unknown molecular pathway underlying the
635 AD-mediated cardiac neuro-signaling dysregulation. Notably, we demonstrated that

636 the cardiac tissue of AD patients with CAA exhibits significantly reduced neurotrophic
637 markers, including BDNF, together with Aβ deposits within the myocardial tissue. The
638 presence of Aβ aggregates was also previously revealed in the human AD heart[9],
639 reinforcing the relevance of our findings.
640 To our knowledge, this is the first study that investigated the impact of Aβ pathology
641 on the neurotrophic signaling pathway in the AD heart and its effect on cardiovascular
642 physiology in an AD animal model, with a validation of the loss of neurotrophic
643 signaling mediators in human AD post-mortem cardiac tissue. These findings uncover
644 a previously unrecognized dysfunction in the BDNF/TrkB/CREB signaling pathway,
645 driven by Aβ accumulation within the cardiac nervous system. This disruption
646 highlights neurotrophic signaling as a promising and novel pharmacological target for
647 combating AD-induced cardiac dysfunction. While further clinical and translational
648 studies are needed to fully validate these conclusions, our results strongly suggest
649 that treating AD-related heart failure (HF) may require a therapeutic strategy
650 specifically aimed at the cardiac neuronal system, one that goes beyond conventional
651 HF pharmacotherapy.
652
653 This emerging perspective calls for deeper investigation into the neuro-cardiac axis in
654 AD. Importantly, our study opens a new translational avenue that may help personalize
655 AD therapy in subjects with cardiac pathology, as well as characterize AD as a multi-
656 organ neurodegenerative syndrome.
657
658 **4.1 Limitations.** While our study provides valuable insights into the cardiac
659 implications of AD, several limitations should be acknowledged. First, we did not
660 assess left ventricular diastolic function in our in vivo model, which has been implicated
661 in previous studies of AD patients demonstrating diastolic impairment correlated with
662 cardiac electrical abnormalities. Of note, given the advanced age of the animals used
663 in the study, some technical difficulties do not always allow for consistent
664 measurement of E/A ratios in all animals, given that the E and A waves overlap at a
665 higher heart rate, as already demonstrated[18]. Therefore, the E/E′ ratio is not always
666 considered a trustworthy measurement to assess the diastolic function in aging in vivo
667 models, as also reported in murine heart failure with preserved ejection fraction and in
668 volume overload models[19]. Accordingly, diastolic dysfunction was computed by
669 using the reverse peak option to evaluate reverse global longitudinal strain (GLS) and

global radial strain (GRS) rates, which were derived from long-axis B-mode traces. Moreover, our focus on systolic function deterioration aligns with findings linking systolic impairment to cerebral hypoperfusion and emboli formation in AD patients, highlighting the connection between Aβ pathology and cardiovascular disease[72]. Additionally, due to the frailty of our AD mouse model and the desire to minimize stress-induced effects, we refrained from performing hemodynamic analysis, which could have provided further insights but may have impacted our animal population adversely[73]. Other neurotrophic factors, such as NT3 and NT4, may also contribute to cardiac innervation and function. Future investigations should explore the potential involvement of these factors in the AD myocardium to provide a comprehensive understanding of the cardiac neuro-signaling dysregulation. The potential of the BDNF/TrkB/CREB signaling reactivation to reverse or prevent cardiac dysfunction remains to be tested in vivo. Studies employing pharmacological strategies to increase cerebral amyloid clearance are also under development[74], to determine if reducing brain amyloid pathology may ameliorate heart function. Additionally, generating AD mouse models with BDNF cardiomyocyte-specific deletion could significantly enhance future research approaches. However, the combined mutations may lead to early morbidity and reduced lifespan[75, 76], therefore careful experimental design and substantial investment in resources and technology will be needed. Furthermore, Aβ plaques exacerbate cellular stress and inflammation, driving degenerative processes across multiple cell types, including neurons and brain endothelial cells. This cascade worsens BBB breakdown and accelerates AD-induced maladaptive remodeling. In our study, we demonstrated that SAA3, a novel inflammatory marker for ischemic heart disease [63-65], predominantly accumulates in the cardiac vessel walls of Tg2576-AD mice, together with Aβ deposits. This suggests that misfolded Aβ peptides or oligomers may infiltrate the vascular system, reaching the heart and fostering the seeding of other systemic amyloid deposition around myocardial vessels. These findings highlight the need for further investigation into the inflammatory dynamics of Alzheimer's heart pathology, an intriguing avenue for future research beyond the scope of this study. Lastly, the sample size of our human cardiac post-mortem specimens is limited, as obtaining human cardiac samples from AD patients without significant cardiovascular diseases is extremely challenging. Future, more comprehensive clinical studies are recommended to confirm AD cardiac dysfunction and validate the Aβ-mediated myocardial denervation observed in our study. Despite

704 these limitations, our findings offer novel key insights into the pathophysiology of AD-
705 related cardiac dysfunction and underscore the need for further research to improve
706 the clinical management of AD patients.
707
708 **5. Conclusions.** In summary, our study elucidates a profound impact of AD amyloid
709 pathology on cardiac function, highlighting the maladaptive cardiac remodeling
710 characterized by amyloid deposition, fibrosis, and a previously unknown dysregulation
711 of the neurotrophic signaling pathway. The study also uncovers a mechanism whereby
712 Aβ-induced reduction in cardiac CREB activation impairs BDNF transcription,
713 ultimately leading to myocardial denervation, pro-apoptotic signaling, and cardiac
714 physiological dysfunction. These findings significantly contribute to our understanding
715 of AD pathophysiology, particularly Aβ-mediated cardiac dysfunction. Moreover, our
716 study identifies potential therapeutic targets within the neurotrophic signaling pathway
717 to mitigate the detrimental effects of AD and amyloid pathology on the cardiovascular
718 system, bridging the gap between molecular insights and potential for clinical
719 translation. Finally, this study underscores the importance of considering cardiac
720 complications in managing AD and offers promising avenues for future research and
721 therapeutic development.

722 **6. Acknowledgement**

723 We acknowledge that Supplementary Figure 9 was created using BioRender.com. We
724 thank the Brain and Body Donation Program Banner Sun Health Research Institute
725 clinical biobank for providing human LV post-mortem tissue. We thank Life Science
726 Editors for editing services.

727 **7. Funding**

728 This work was supported by NIH R01NS104127 and R01AG062572 grants, the
729 Alzheimer's Association (AARG-20-685663), and the Pennsylvania Department of
730 Health Collaborative Research on Alzheimer's Disease (PA Cure) Grant awarded to
731 SF, by the NIH SC1GM128210 grant awarded to SJ, by American Heart Association
732 Postdoctoral fellowship 24POST1240115 awarded to AE, by the Karen Toffler
733 Charitable Trust, and the Lemole Center for Integrated Lymphatics research.

734 **8. Authors Contribution**

AE and SF designed the study. AE performed and conceptualized the experiments and analyzed the data. AE wrote the paper draft and did the literature search. RPR, AC, and RVT performed experiments. SF provided relevant insights, scientific supervision, critically revised the manuscript and acquired funding. SJ revised the study, edited the manuscript, offered additional literature searches.

9. Conflict of interest

The authors declare no conflicts of interest.

10. Data availability

The corresponding author will share the data underlying this article upon reasonable request.

11. References

1. Hebert, L.E., et al., *Alzheimer disease in the United States (2010-2050) estimated using the 2010 census.* Neurology, 2013. **80**(19): p. 1778-83.
2. Greenberg, S.M., et al., *Cerebral amyloid angiopathy and Alzheimer disease - one peptide, two pathways.* Nat Rev Neurol, 2020. **16**(1): p. 30-42.
3. Masters, C.L., et al., *Alzheimer's disease.* Nat Rev Dis Primers, 2015. **1**: p. 15056.
4. Sanna, G.D., et al., *Cardiac Abnormalities in Alzheimer Disease: Clinical Relevance Beyond Pathophysiological Rationale and Instrumental Findings?* JACC Heart Fail, 2019. **7**(2): p. 121-128.
5. Carey, A. and S. Fossati, *Hypertension and hyperhomocysteinemia as modifiable risk factors for Alzheimer's disease and dementia: New evidence, potential therapeutic strategies, and biomarkers.* Alzheimers Dement, 2023. **19**(2): p. 671-695.
6. Hachinski, V., et al., *Preventing dementia by preventing stroke: The Berlin Manifesto.* Alzheimers Dement, 2019. **15**(7): p. 961-984.
7. Saeed, A., et al., *Cardiovascular Disease and Alzheimer's Disease: The Heart-Brain Axis.* J Am Heart Assoc, 2023. **12**(21): p. e030780.
8. Luciani, M., et al., *Big tau aggregation disrupts microtubule tyrosination and causes myocardial diastolic dysfunction: from discovery to therapy.* Eur Heart J, 2023. **44**(17): p. 1560-1570.
9. Troncone, L., et al., *Abeta Amyloid Pathology Affects the Hearts of Patients With Alzheimer's Disease: Mind the Heart.* J Am Coll Cardiol, 2016. **68**(22): p. 2395-2407.
10. Allen, S.J., J.J. Watson, and D. Dawbarn, *The neurotrophins and their role in Alzheimer's disease.* Curr Neuropharmacol, 2011. **9**(4): p. 559-73.
11. Garzon, D., G. Yu, and M. Fahnestock, *A new brain-derived neurotrophic factor transcript and decrease in brain-derived neurotrophic factor transcripts 1, 2 and 3 in Alzheimer's disease parietal cortex.* J Neurochem, 2002. **82**(5): p. 1058-64.
12. Matthews, V.B., et al., *Brain-derived neurotrophic factor is produced by skeletal muscle cells in response to contraction and enhances fat oxidation via activation of AMP-activated protein kinase.* Diabetologia, 2009. **52**(7): p. 1409-18.
13. Kermani, P. and B. Hempstead, *BDNF Actions in the Cardiovascular System: Roles in Development, Adulthood and Response to Injury.* Front Physiol, 2019. **10**: p. 455.

14. Cannavo, A., et al., *beta3AR-Dependent Brain-Derived Neurotrophic Factor (BDNF) Generation Limits Chronic Postischemic Heart Failure.* Circ Res, 2023. **132**(7): p. 867-881.
15. Hsiao, K., et al., *Correlative memory deficits, Abeta elevation, and amyloid plaques in transgenic mice.* Science, 1996. **274**(5284): p. 99-102.
16. Robbins, E.M., et al., *Kinetics of cerebral amyloid angiopathy progression in a transgenic mouse model of Alzheimer disease.* J Neurosci, 2006. **26**(2): p. 365-71.
17. Rigaud, V.O., et al., *UCP2 modulates cardiomyocyte cell cycle activity, acetyl-CoA, and histone acetylation in response to moderate hypoxia.* JCI Insight, 2022. **7**(15).
18. de Lucia, C., et al., *Echocardiographic Strain Analysis for the Early Detection of Left Ventricular Systolic/Diastolic Dysfunction and Dyssynchrony in a Mouse Model of Physiological Aging.* J Gerontol A Biol Sci Med Sci, 2019. **74**(4): p. 455-461.
19. Schnelle, M., et al., *Echocardiographic evaluation of diastolic function in mouse models of heart disease.* J Mol Cell Cardiol, 2018. **114**: p. 20-28.
20. Cannavo, A., et al., *Aldosterone Jeopardizes Myocardial Insulin and beta-Adrenergic Receptor Signaling via G Protein-Coupled Receptor Kinase 2.* Front Pharmacol, 2019. **10**: p. 888.
21. de Lucia, C., et al., *Long-Term Caloric Restriction Improves Cardiac Function, Remodeling, Adrenergic Responsiveness, and Sympathetic Innervation in a Model of Postischemic Heart Failure.* Circ Heart Fail, 2018. **11**(3): p. e004153.
22. Elia, A., et al., *Aging is associated with cardiac autonomic nerve fiber depletion and reduced cardiac and circulating BDNF levels.* J Geriatr Cardiol, 2021. **18**(7): p. 549-559.
23. Marzano, F., et al., *Genetic Catalytic Inactivation of GRK5 Impairs Cardiac Function in Mice Via Dysregulated P53 Levels.* JACC Basic Transl Sci, 2022. **7**(4): p. 366-380.
24. Fossati, S., et al., *The carbonic anhydrase inhibitor methazolamide prevents amyloid beta-induced mitochondrial dysfunction and caspase activation protecting neuronal and glial cells in vitro and in the mouse brain.* Neurobiol Dis, 2016. **86**: p. 29-40.
25. Davidson, M.M., et al., *Novel cell lines derived from adult human ventricular cardiomyocytes.* J Mol Cell Cardiol, 2005. **39**(1): p. 133-47.
26. Lippi, M., et al., *Human Cell Modeling for Cardiovascular Diseases.* Int J Mol Sci, 2020. **21**(17).
27. Grimm, M.O.W., et al., *The impact of capsaicinoids on APP processing in Alzheimer's disease in SH-SY5Y cells.* Sci Rep, 2020. **10**(1): p. 9164.
28. Koriyama, Y., et al., *Glyceraldehyde caused Alzheimer's disease-like alterations in diagnostic marker levels in SH-SY5Y human neuroblastoma cells.* Sci Rep, 2015. **5**: p. 13313.
29. Riegerova, P., et al., *Expression and Localization of AbetaPP in SH-SY5Y Cells Depends on Differentiation State.* J Alzheimers Dis, 2021. **82**(2): p. 485-491.
30. Schwarzbauer, J.E. and D.W. DeSimone, *Fibronectins, their fibrillogenesis, and in vivo functions.* Cold Spring Harb Perspect Biol, 2011. **3**(7).
31. Aishwarya, R., et al., *Diastolic dysfunction in Alzheimer's disease model mice is associated with Abeta-amyloid aggregate formation and mitochondrial dysfunction.* Sci Rep, 2024. **14**(1): p. 16715.
32. Kawarabayashi, T., et al., *Age-dependent changes in brain, CSF, and plasma amyloid (beta) protein in the Tg2576 transgenic mouse model of Alzheimer's disease.* J Neurosci, 2001. **21**(2): p. 372-81.
33. Kuo, Y.M., et al., *Elevated abeta42 in skeletal muscle of Alzheimer disease patients suggests peripheral alterations of AbetaPP metabolism.* Am J Pathol, 2000. **156**(3): p. 797-805.
34. Tublin, J.M., et al., *Getting to the Heart of Alzheimer Disease.* Circ Res, 2019. **124**(1): p. 142-149.
35. Fossati, S., J. Ghiso, and A. Rostagno, *TRAIL death receptors DR4 and DR5 mediate cerebral microvascular endothelial cell apoptosis induced by oligomeric Alzheimer's Abeta.* Cell Death Dis, 2012. **3**(6): p. e321.

36. Parodi-Rullan, R., et al., *Alzheimer's amyloid beta heterogeneous species differentially affect brain endothelial cell viability, blood-brain barrier integrity, and angiogenesis.* Aging Cell, 2020. **19**(11): p. e13258.
37. Dobson, C.M., *Principles of protein folding, misfolding and aggregation.* Semin Cell Dev Biol, 2004. **15**(1): p. 3-16.
38. De Buck, M., et al., *Structure and Expression of Different Serum Amyloid A (SAA) Variants and their Concentration-Dependent Functions During Host Insults.* Curr Med Chem, 2016. **23**(17): p. 1725-55.
39. den Hartigh, L.J., et al., *Serum amyloid A and metabolic disease: evidence for a critical role in chronic inflammatory conditions.* Front Cardiovasc Med, 2023. **10**: p. 1197432.
40. Arancio, O. and M.V. Chao, *Neurotrophins, synaptic plasticity and dementia.* Curr Opin Neurobiol, 2007. **17**(3): p. 325-30.
41. Nasrolahi, A., et al., *Therapeutic potential of neurotrophic factors in Alzheimer's Disease.* Mol Biol Rep, 2022. **49**(3): p. 2345-2357.
42. Du, Y., et al., *Postmortem Brain, Cerebrospinal Fluid, and Blood Neurotrophic Factor Levels in Alzheimer's Disease: A Systematic Review and Meta-Analysis.* J Mol Neurosci, 2018. **65**(3): p. 289-300.
43. Esvald, E.E., et al., *CREB Family Transcription Factors Are Major Mediators of BDNF Transcriptional Autoregulation in Cortical Neurons.* J Neurosci, 2020. **40**(7): p. 1405-1426.
44. Garzon, D.J. and M. Fahnestock, *Oligomeric amyloid decreases basal levels of brain-derived neurotrophic factor (BDNF) mRNA via specific downregulation of BDNF transcripts IV and V in differentiated human neuroblastoma cells.* J Neurosci, 2007. **27**(10): p. 2628-35.
45. Massa, S.M., et al., *Small molecule BDNF mimetics activate TrkB signaling and prevent neuronal degeneration in rodents.* J Clin Invest, 2010. **120**(5): p. 1774-85.
46. Anzovino, A., et al., *Amyloid Beta Oligomers Activate Death Receptors and Mitochondria-Mediated Apoptotic Pathways in Cerebral Vascular Smooth Muscle Cells; Protective Effects of Carbonic Anhydrase Inhibitors.* Cells, 2023. **12**(24).
47. Cazorla, M., et al., *Identification of a low-molecular weight TrkB antagonist with anxiolytic and antidepressant activity in mice.* J Clin Invest, 2011. **121**(5): p. 1846-57.
48. Tahsili-Fahadan, P. and R.G. Geocadin, *Heart-Brain Axis: Effects of Neurologic Injury on Cardiovascular Function.* Circ Res, 2017. **120**(3): p. 559-572.
49. Elia, A. and S. Fossati, *Autonomic nervous system and cardiac neuro-signaling pathway modulation in cardiovascular disorders and Alzheimer's disease.* Front Physiol, 2023. **14**: p. 1060666.
50. Ihara, M. and K. Washida, *Linking Atrial Fibrillation with Alzheimer's Disease: Epidemiological, Pathological, and Mechanistic Evidence.* J Alzheimers Dis, 2018. **62**(1): p. 61-72.
51. Cermakova, P., et al., *Heart failure and Alzheimer's disease.* J Intern Med, 2015. **277**(4): p. 406-25.
52. Kramer, L.M., et al., *Amyloid precursor protein-fragments-containing inclusions in cardiomyocytes with basophilic degeneration and its association with cerebral amyloid angiopathy and myocardial fibrosis.* Sci Rep, 2018. **8**(1): p. 16594.
53. Cade, S., X.F. Zhou, and L. Bobrovskaya, *The role of brain-derived neurotrophic factor and the neurotrophin receptor p75NTR in age-related brain atrophy and the transition to Alzheimer's disease.* Rev Neurosci, 2022. **33**(5): p. 515-529.
54. Gao, L., et al., *Brain-derived neurotrophic factor in Alzheimer's disease and its pharmaceutical potential.* Transl Neurodegener, 2022. **11**(1): p. 4.
55. Vitaliano, G.D., et al., *Clathrin-nanoparticles deliver BDNF to hippocampus and enhance neurogenesis, synaptogenesis and cognition in HIV/neuroAIDS mouse model.* Commun Biol, 2022. **5**(1): p. 236.
56. Wang, C.S., E.T. Kavalali, and L.M. Monteggia, *BDNF signaling in context: From synaptic regulation to psychiatric disorders.* Cell, 2022. **185**(1): p. 62-76.

57. Ghiso, J., S. Fossati, and A. Rostagno, *Amyloidosis associated with cerebral amyloid angiopathy: cell signaling pathways elicited in cerebral endothelial cells.* J Alzheimers Dis, 2014. **42 Suppl 3**(0 3): p. S167-76.
58. Hanon, O., et al., *Plasma amyloid beta predicts conversion to dementia in subjects with mild cognitive impairment: The BALTAZAR study.* Alzheimers Dement, 2022. **18**(12): p. 2537-2550.
59. Zicha, S., et al., *Comparative analytical performance of multiple plasma Abeta42 and Abeta40 assays and their ability to predict positron emission tomography amyloid positivity.* Alzheimers Dement, 2023. **19**(3): p. 956-966.
60. Ulm, B.S., D.R. Borchelt, and B.D. Moore, *Remodeling Alzheimer-amyloidosis models by seeding.* Mol Neurodegener, 2021. **16**(1): p. 8.
61. Jang, S., et al., *Beta-Amyloid Instigates Dysfunction of Mitochondria in Cardiac Cells.* Cells, 2022. **11**(3).
62. Parodi-Rullan, R.M., S. Javadov, and S. Fossati, *Dissecting the Crosstalk between Endothelial Mitochondrial Damage, Vascular Inflammation, and Neurodegeneration in Cerebral Amyloid Angiopathy and Alzheimer's Disease.* Cells, 2021. **10**(11).
63. Chait, A., et al., *Sexually Dimorphic Relationships Among Saa3 (Serum Amyloid A3), Inflammation, and Cholesterol Metabolism Modulate Atherosclerosis in Mice.* Arterioscler Thromb Vasc Biol, 2021. **41**(6): p. e299-e313.
64. Johnson, B.D., et al., *Serum amyloid A as a predictor of coronary artery disease and cardiovascular outcome in women: the National Heart, Lung, and Blood Institute-Sponsored Women's Ischemia Syndrome Evaluation (WISE).* Circulation, 2004. **109**(6): p. 726-32.
65. Morrow, D.A., et al., *Serum amyloid A predicts early mortality in acute coronary syndromes: A TIMI 11A substudy.* J Am Coll Cardiol, 2000. **35**(2): p. 358-62.
66. Rissman, R.A., et al., *Caspase-cleavage of tau is an early event in Alzheimer disease tangle pathology.* J Clin Invest, 2004. **114**(1): p. 121-30.
67. Conze, C., et al., *Caspase-cleaved tau is senescence-associated and induces a toxic gain of function by putting a brake on axonal transport.* Mol Psychiatry, 2022. **27**(7): p. 3010-3023.
68. Hoth, K.F., et al., *Cardiac dysfunction and cognition in older adults with heart failure.* Cogn Behav Neurol, 2008. **21**(2): p. 65-72.
69. Numakawa, T. and H. Odaka, *The Role of Neurotrophin Signaling in Age-Related Cognitive Decline and Cognitive Diseases.* Int J Mol Sci, 2022. **23**(14).
70. Bahls, M., et al., *Brain-derived neurotrophic factor is related with adverse cardiac remodeling and high NTproBNP.* Sci Rep, 2019. **9**(1): p. 15421.
71. Takashio, S., et al., *Significance of low plasma levels of brain-derived neurotrophic factor in patients with heart failure.* Am J Cardiol, 2015. **116**(2): p. 243-9.
72. Tini, G., et al., *Alzheimer's Disease and Cardiovascular Disease: A Particular Association.* Cardiol Res Pract, 2020. **2020**: p. 2617970.
73. Miranda-Silva, D., et al., *Assessing Rodent Cardiac Function in vivo Using Hemodynamic Pressure-Volume Loops.* Front Physiol, 2021. **12**: p. 751326.
74. Canepa, E., et al., *FDA-approved carbonic anhydrase inhibitors reduce amyloid beta pathology and improve cognition, by ameliorating cerebrovascular health and glial fitness.* Alzheimers Dement, 2023. **19**(11): p. 5048-5073.
75. Jankowsky, J.L. and H. Zheng, *Practical considerations for choosing a mouse model of Alzheimer's disease.* Mol Neurodegener, 2017. **12**(1): p. 89.
76. Zhong, M.Z., et al., *Updates on mouse models of Alzheimer's disease.* Mol Neurodegener, 2024. **19**(1): p. 23.
77. Jang, S.W., et al., *Deoxygedunin, a natural product with potent neurotrophic activity in mice.* PLoS One, 2010. **5**(7): p. e11528.
78. Jang, S.W., et al., *A selective TrkB agonist with potent neurotrophic activities by 7,8-dihydroxyflavone.* Proc Natl Acad Sci U S A, 2010. **107**(6): p. 2687-92.

929 79. Wang, Z., et al., *Brain-derived neurotrophic factor mimetic, 7,8-dihydroxyflavone, protects*
930 *against myocardial ischemia by rebalancing optic atrophy 1 processing.* Free Radic Biol Med,
931 2019. **145**: p. 187-197.

932

Figures

Figure 1

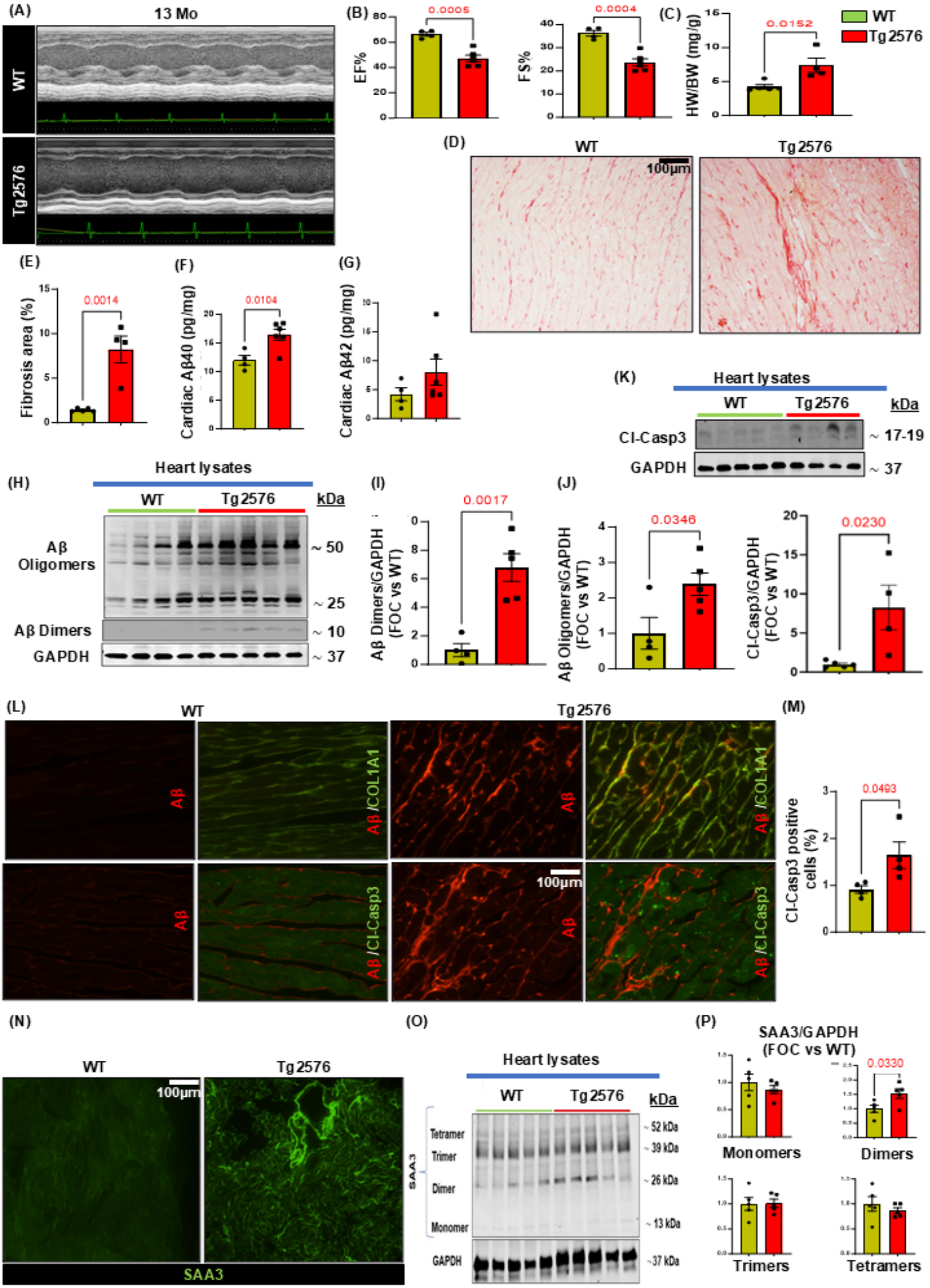

934 **Figure 1. Cardiac physiological impairment, myocardial Aβ aggregates**
935 **accumulation, cardiac cell apoptosis and Serum amyloid A3 (SAA3) deposition**
936 **in the heart of Tg2576 AD mice.** (**A**) M-mode representative images of
937 echocardiographic analysis in 13-month-old WT and Tg2576 mice. (**B**) Left ventricle
938 (LV) function is impaired in the AD model, as evidenced by a significant decline both
939 in ejection fraction (EF%) and fraction shortening percentage (FS%) showed by the
940 Tg2576 group compared to WT mice age-matched (13-months-old). (**C**) The heart
941 weight/body weight ratio is significantly increased in Tg2576 mice compared to the WT
942 group. (**D**-**E**) Representative images (left panels) and quantitative data (right panels)
943 showing the percentage (%) of fibrotic area in cardiac sections from WT and Tg2576
944 mice, assessed via Picrosirius red staining (scale bar 50μm). (**F**-**G**): Aβ40 (**F**) Aβ42
945 (**G**) cardiac levels (pg/mg of proteins), assessed by ELISA assay, in total cardiac
946 lysates from WT and Tg2576 mice. (**H**-**J**): Representative immunoblots (left panels)
947 and densitometric quantitative analysis (right panels) showing protein levels of Aβ
948 dimers, oligomers (**I**-**J**) in total cardiac lysates from WT and Tg2576 mice. GAPDH
949 levels were used as a loading control. (**K**): Representative immunoblots (upper panels)
950 and densitometric quantitative analysis (lower panels) showing protein levels of
951 Cleaved-Caspase3 (Cl-Casp3) in total cardiac lysates from WT and Tg2576 mice.
952 GAPDH levels were used as a loading control. (**L**): Representative digital images
953 (upper panels, scale bar 100μm) showing collagen type I fibers (COL1A1, in green)
954 and Aβ (in red) and representative digital images (lower panels; scale bar 100μm) and
955 quantification (**M**) showing Cleaved-Caspase3 (Cl-Casp3, in green) and Aβ (in red) in
956 cardiac sections from WT and Tg2576 mice. (**N**): Representative WT and Tg2576
957 cardiac sections stained for serum amyloid A3 (SAA3, in green, scale bar 100μm). (**O**-
958 **P**): Representative immunoblots (**O**) and densitometric quantitative analysis (**P**)
959 showing levels of different aggregates of SAA3 in total cardiac lysates from WT and
960 Tg2576 mice. GAPDH levels were used as a loading control. n=4-6 mice/group. Data
961 are presented as a mean±SEM. *P<0.05 and vs WT. Student t-tests were performed
962 between the groups.

963

964

965

Figure 2

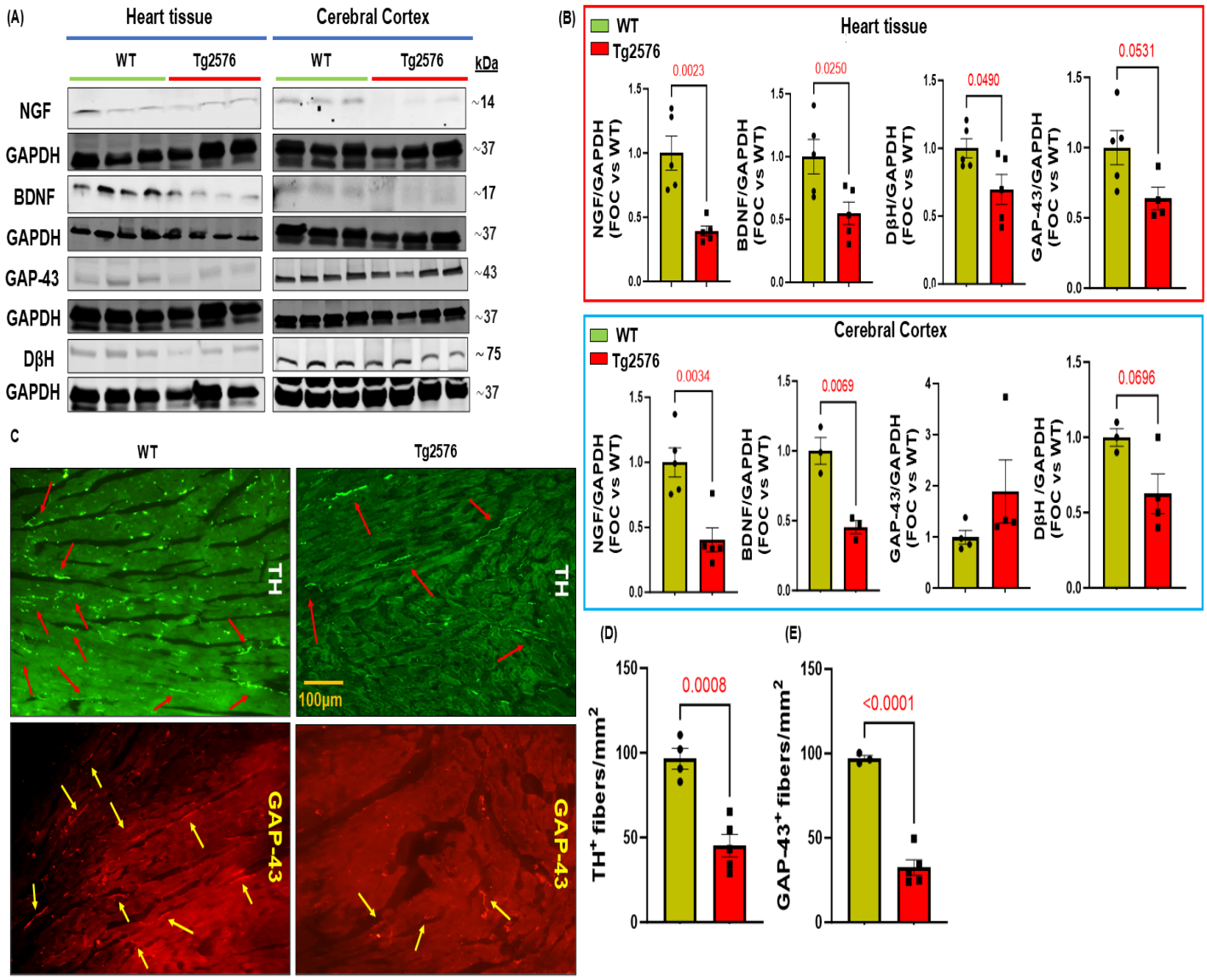

Figure 2. Alzheimer's disease pathology negatively impacts the neuro-signaling pathway in the brain/heart axis of Tg2576 mice. (**A**-**B**): Representative immunoblots (**A**) and densitometric analysis (**B**) showing levels of NGF, BDNF, GAP-43, and dβh in total heart tissue and cerebral cortex lysates from WT and Tg2576 mice. GAPDH levels were used as a loading control. (**C**-**E**): Digital images (**C**, scale bar 100µm) and quantifications (**D**-**E**) showing cardiac adrenergic nerve fibers, labeled with anti-tyrosine-hydroxylase (TH, in green) (**D**), and cardiac regenerating nerve endings, labeled with anti-neuronal regeneration marker (GAP-43, in red) (**E**), in cardiac sections from WT and Tg2576 mice. n=3-5 mice/group. Data are presented as a mean±SEM. *P<0.05 and vs WT. Student t-tests have been performed between the groups.

Figure 3

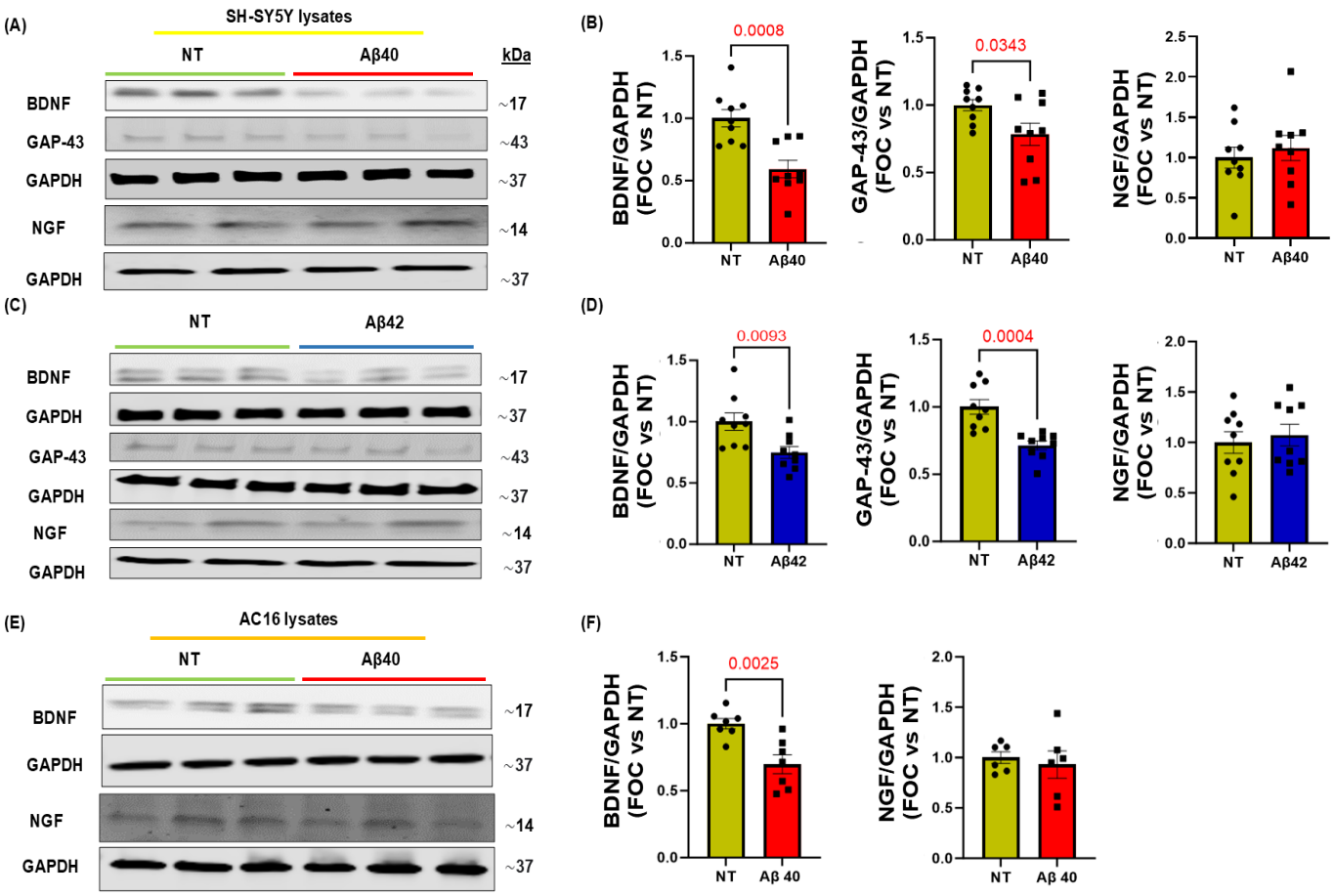

Figure 3. Effects of human Aβ40 or Aβ42 oligomers on neurotrophic factors in neuronal cells (SH-SY5Y) and human cardiomyocytes (AC16). (**A-D**): Representative immunoblots (**A-C**) and densitometric analysis (**B-D**) of multiple independent experiments to evaluate BDNF, NGF, and GAP-43 protein levels (**B-D**) in human neuroblastoma cells (SH-SY5Y) stimulated with human Aβ40 or Aβ42 oligomers for 16 h. GAPDH levels were used as a loading control. (**E-F**): Representative immunoblots (**E**) and densitometric quantitative analysis (**F**) showing protein levels of BDNF and NGF in total protein lysates from human cardiomyocytes (AC16) stimulated with human Aβ40 oligomers for 16 h. GAPDH levels were used as a loading control. n=6-9. Data are presented as a mean±SEM. *P<0.05 and vs NT. Student t-tests have been performed between the groups. (NT= Not Treated).

Figure 4

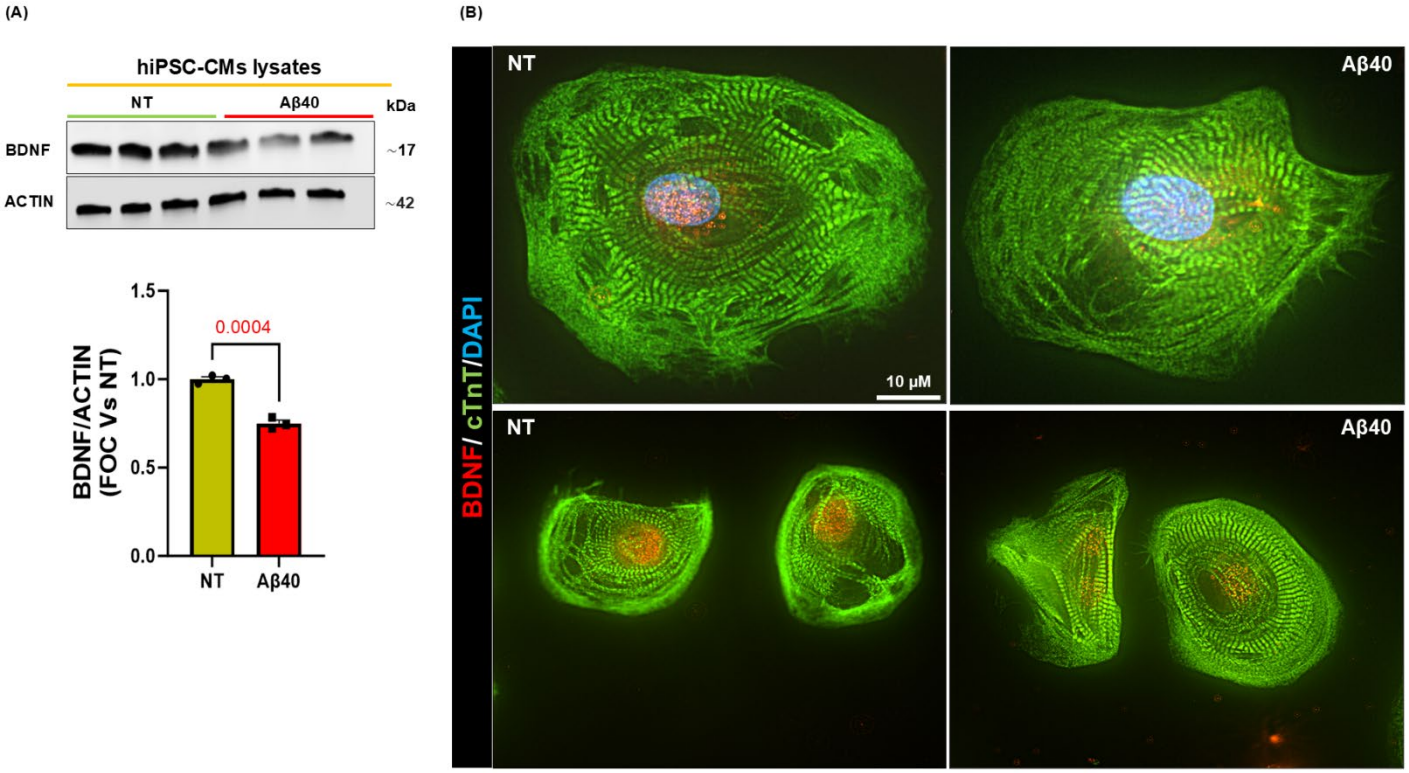

992

993 **Figure 4. Aβ40 oligomers induce BDNF downregulation in human-induced**
994 **pluripotent stem cell-derived cardiomyocytes (hiPSC-CMs).** (**A**) Representative
995 immunoblots (upper panels) and densitometric quantitative analysis (lower panel)
996 showing protein levels of BDNF in total protein lysates from hiPSC-CMs stimulated
997 with human Aβ40 oligomers for 20h. ACTIN levels were used as loading control. (**B**)
998 Representative digital images (scale bar 10µm) of hiPSC-CMs stained with BDNF
999 (red), cardiac Troponin T (cTnT, in green), and DAPI (blue).n=3. Data are presented
1000 as a mean±SEM. *P<0.05 and vs NT. Student t-tests have been performed between
1001 the groups. (NT= Not Treated).

1002

1003

1004

1005

1006

1007

Figure 5

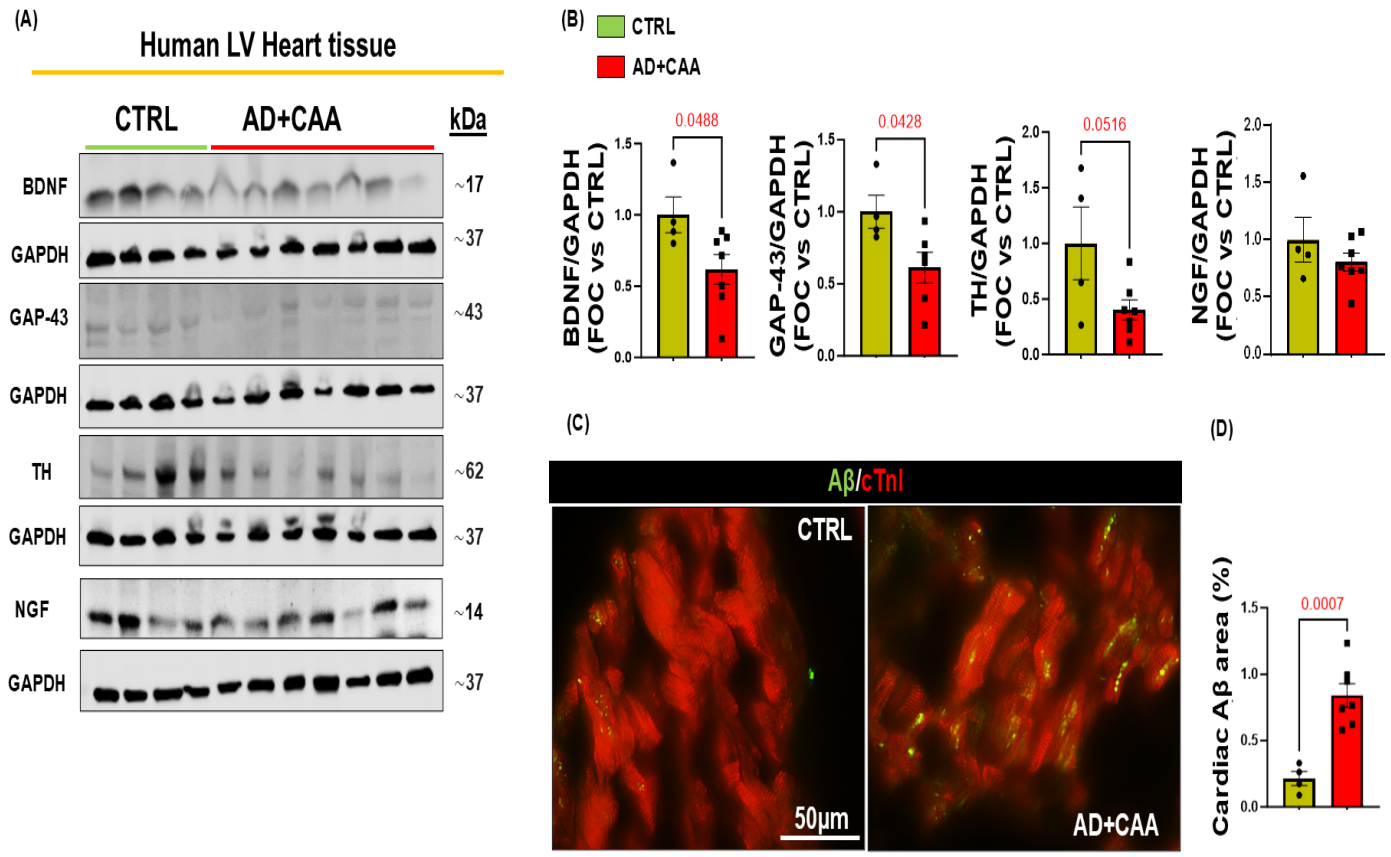

1008

1009 **Figure 5. Myocardial neuro-signaling impairment and Aβ deposits in human**
1010 **post-mortem cardiac tissue of AD subjects.** (**A-B**): Representative immunoblots
1011 (**A**) and densitometric analysis (**B**) showing reduced levels of BDNF, GAP-43, TH, but
1012 not NGF in total human LV lysates of patients with AD+CAA compared to healthy
1013 donors (CTRL). GAPDH levels were used as a loading control. (**C-D**): Representative
1014 digital images (**C**, scale bar 50µm), and quantification (**D**) of the LV sections from
1015 CTRL and AD+CAA subjects stained with Aβ aggregates (in green) and cardiac
1016 Troponin I (cTnI, in red). n=4-7 subjects/group. Data are presented as a mean±SEM.
1017 *P<0.05 and vs CTRL. Student t-tests have been performed between the groups.

1018

1019

1020

1021

Figure 6

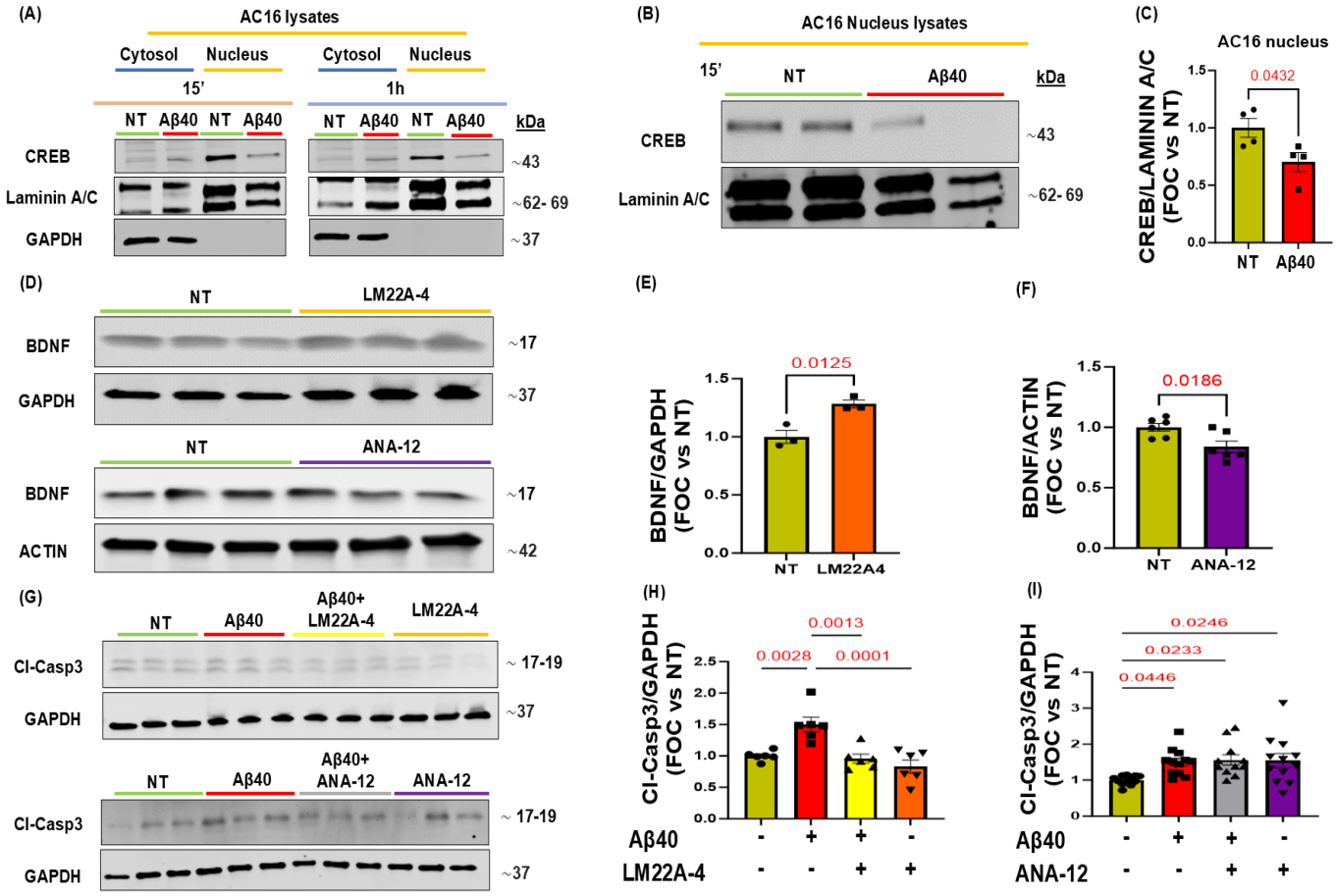

Figure 6. CREB signaling is impaired by Aβ40 oligomers and a TrkB agonist reduces Aβ40-mediated caspase 3 activation in human cardiomyocytes (AC16 cells). (**A-C**): Representative immunoblots (**A-B**) and densitometric quantitative analysis (**C**) of multiple independent experiments to evaluate CREB levels in nuclear extracts isolated from human cardiomyocytes (AC16) stimulated with human Aβ-40 oligomers for 15 minutes or 1h. LAMININ A/C levels were used as a nuclear loading control. (**D-F**): Representative immunoblots (**D**) and densitometric quantitative analysis (**E-F**) showing protein levels of BDNF in total protein lysates from human cardiomyocytes (AC16) stimulated with TrkB agonist LM22A-4 (100 nM) or TrkB antagonist ANA-12 (30 μM) for 16 h. GAPDH and ACTIN levels were used as loading controls. n=3-6. Data are presented as a mean±SEM. *P<0.05 and vs NT. Student t-tests have been performed between the groups. (**G-I**): Representative immunoblots (**G**) and densitometric quantitative analysis (**H-I**) of multiple independent experiments to evaluate Cleaved-Caspase 3 (Cl-Casp3) in AC16 cells stimulated with human Aβ-40 oligomers for 16 h. Before Aβ-40 oligomers treatment, cells were pretreated with

1038 either LM22A-4 (100 nM, top panel), or ANA-12 (30 μM, bottom panel) for 1 h. GAPDH
1039 levels were used as a loading control. n=6-12. One-way ANOVA with Tukey's multiple
1040 comparisons post hoc test: *P<0.05 and vs NT. (NT= Not Treated).

1041

Table 1

Demographic features of the individual cases from the clinical population.

Age	Ethnicity /Gender	Group	Associated Diseases and Comorbidities
53	CM	CTRL	Adenocarcinoma, Status post-Whipple procedure and liver transplantation, Hydroceles, Pulmonary vascular congestion, Hepatic congestion
75	CM	CTRL	Renal collecting duct carcinoma, Status post-Whipple procedure with gastric bypass and cholecystectomy, Mild cardiomegaly, Aorta Atherosclerosis, Testicular atrophy
81	CM	CTRL	Prostatic adenocarcinoma, Bilateral end-stage lung with honeycombing fibrosis (idiopathic pulmonary fibrosis with bronchiectasis by history), Cardiomegaly with left ventricular myocardial hypertrophy, Hepatomegaly, Hepatitis, Acute tubulointerstitial nephritis
90	CF	CTRL	Bilateral renal atrophy with mild nephrosclerosis and cortical cysts, Generalized atherosclerosis, Chronic esophagitis, Cardiomegaly with left ventricular myocardial hypertrophy, Hepatic centrilobular congestion, Chronic thyroiditis
74	CF	AD+CAA	Clear cell renal cell carcinoma, Cardiomegaly with left ventricular myocardial hypertrophy, Atherosclerosis, thoracic and abdominal aorta; Pulmonary vascular congestion; Hepatic atrophy; Status post thyroidectomy; Status post hysterectomy and bilateral salpingo-oophorectomy
85	CM	AD+CAA	History of prostatic carcinoma, status post prostatectomy, Aortic atherosclerosis, Left ventricular myocardial hypertrophy, Pulmonary fibrosis and bronchiolar metaplasia, Chronic esophagitis, Benign renal cysts, bilateral, Pancreatic and Testicular atrophy, Thyroid Nodular goiter, Status post cholecystectomy and Status post appendectomy
86	CF	AD+CAA	Acute bronchopneumonia, Mild cardiomegaly with left ventricular myocardial hypertrophy, Aortic atherosclerosis, Benign endometrial polyp, Nodular goiter, Osteopenia, Hepatic chronic passive congestion, Enchondroma, lumbar vertebra, Renal cortical cysts, History of plasmacytoma
87	CM	AD+CAA	Acute bronchopneumonia; Pulmonary interstitial fibrosis, Cardiomegaly with left ventricular myocardial hypertrophy, Aortic atherosclerosis, Chronic pyelonephritis, Bilateral renal atrophy, Hepatic atrophy, Cholelithiasis, Parathyroid adenoma, S/P radical prostatectomy, history of prostate cancer, S/P cardiac pacemaker placement
87	CM	AD+CAA	Acute bronchopneumonia, Aortic atherosclerosis, Hepatic chronic passive congestion, Prostatic glandular hyperplasia, Testicular atrophy, Mild chronic thyroiditis, Status post cardiac pacemaker, Diverticulosis, Benign renal cortical cyst, right
89	CF	AD+CAA	Acute bronchopneumonia, Calcified granuloma, Aortic atherosclerosis, Pleural fibrotic plaque, Mild calcification, aortic valve, Atherosclerotic stenosis, Cardiomegaly, Hepatic atrophy, Mild chronic lymphocytic thyroiditis, Status post hysterectomy and bilateral salpingo-oophorectomy
90	CF	AD+CAA	Pancreatic ductal adenocarcinoma, Cardiomegaly, Atherosclerosis, thoracic and abdominal aorta, Emphysema, Diverticulosis, Hashimoto's thyroiditis, Status post supracervical hysterectomy, Benign atrophic and fibrotic breast tissue, Osteopenia

1042

1043 **Table 1. Anatomopathological and demographic characteristics of the selected**
1044 **clinical cohort.** *P values of the patients age = 0.1253 vs CTRL. Student t-tests have
1045 been performed between the groups. **Abbreviations**: **CF**= Caucasian Female, **CM**=
1046 Caucasian Male, **Ctrl**= Control, **AD**= Alzheimer's Disease, **CAA**= Cerebral Amyloid
1047 Angiopathy.

1048

1049

1050

1051

Supplemental Table 1

Echocardiographic analysis	13 months old	
Parameters	**WT**	**Tg2576**
Heart rate (bpm)	446.75±26.25	444.44±32.49
LVEDD (mm)	3.99±0.39	4.54±0.33
LVESD (mm)	2.54±0.21	3.47±0.33**
LVEDV (µl)	71.62±14.59	95.44±16.43
LVESV (µl)	24.13±4.40	50.58±12.00**
EF (%)	66.34±2.68	47.24±5.60***
FS (%)	36.23±2.18	23,70±3.38***
LVAW;d (mm)	0.86±0.10	0.98±0.25
LVAW;s (mm)	1.21±0.21	1,37±0,35
LVPW;d (mm)	1.11±0.15	0.72±0.14**
LVPW;s (mm)	1.53±0.18	1.00±0.12**
LV Mass AW (mg)	155.33±26.40	159.41±37.63
Cardiac output (ml/min)	14.42±1.28	14.75±2.81

Supplemental Table 1. Echocardiographic evaluation. Conventional echocardiographic parameters were measured in 13-month-old WT and Tg2576 mice: heart rate, left ventricular (LV) end diastolic diameter (LVEDD), end systolic diameter (LVESD), end-diastolic volume (LVEDV), end systolic volume (LVESV), ejection fraction (EF), fractional shortening (FS), anterior wall in diastole (LVAW;d) and systole (LVAW;s), posterior wall in diastole (LVPW;d) and systole (LVPW;s), mass of the anterior wall (LV Mass AW), and cardiac output. n=4-6 mice/group. Data are presented as a mean±SEM. *P<0.05, **p<0.01, and ***p<0.001 vs WT. Student t-tests were performed between the groups.

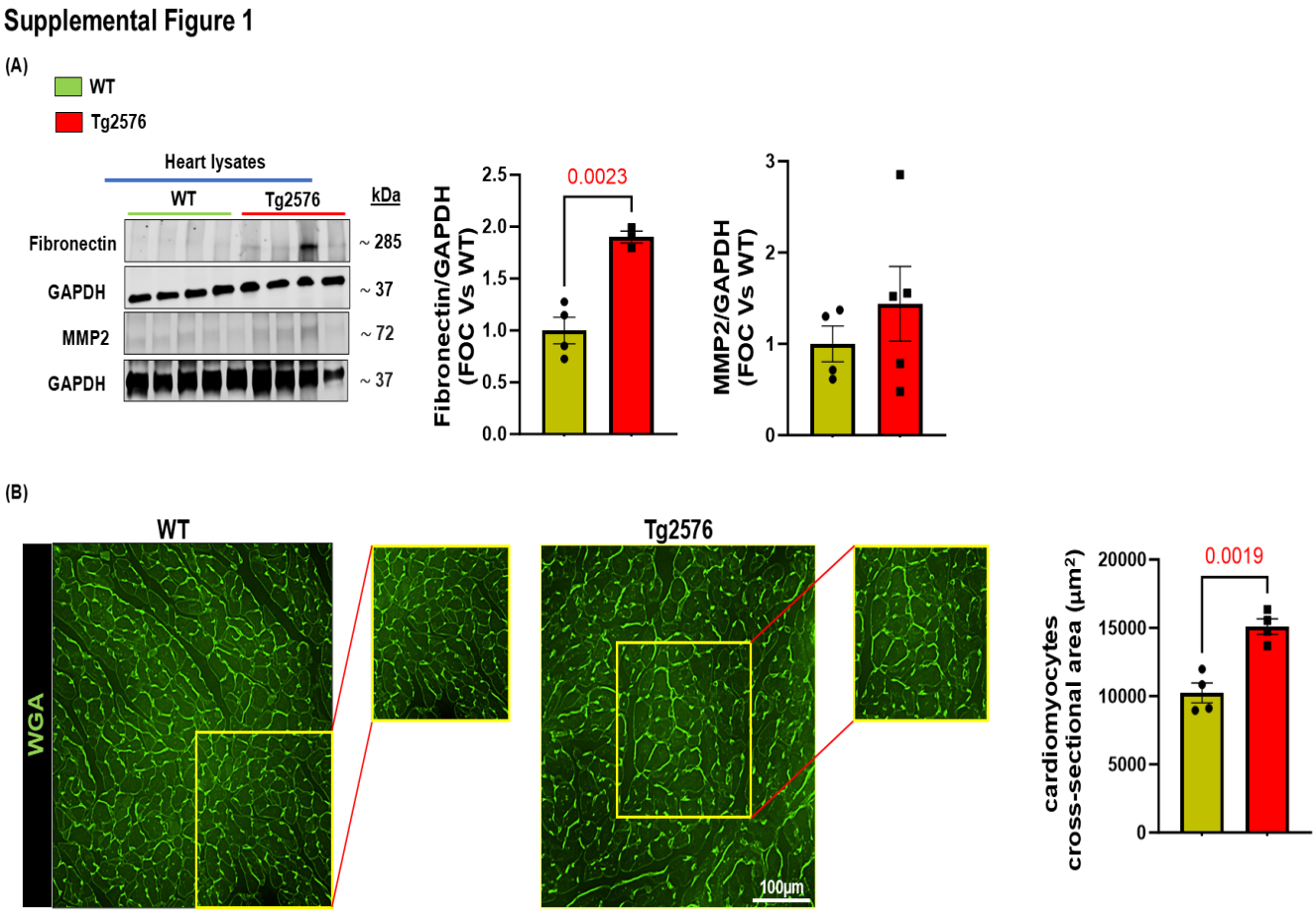

Supplemental Figure 1. Cardiac adverse remodeling in 13-month-old Tg2576-AD mouse heart. (**A**) Representative immunoblots (left panels) and densitometric quantitative analysis (right panels) showing protein levels of fibronectin and MMP2 in total cardiac lysates from WT and Tg2576 mice. GAPDH levels were used as a loading control. (**B**) Representative digital images (left panels, scale bar 100µm), and quantification (right panel) of the cardiomyocyte cross-sectional area (CSA) in cardiac sections from WT and Tg2576 mice stained with WGA. n=4-5 mice/group. Data are presented as a mean±SEM. *P<0.05 and vs WT. Student t-tests have been performed between the groups.

Supplemental Figure 2

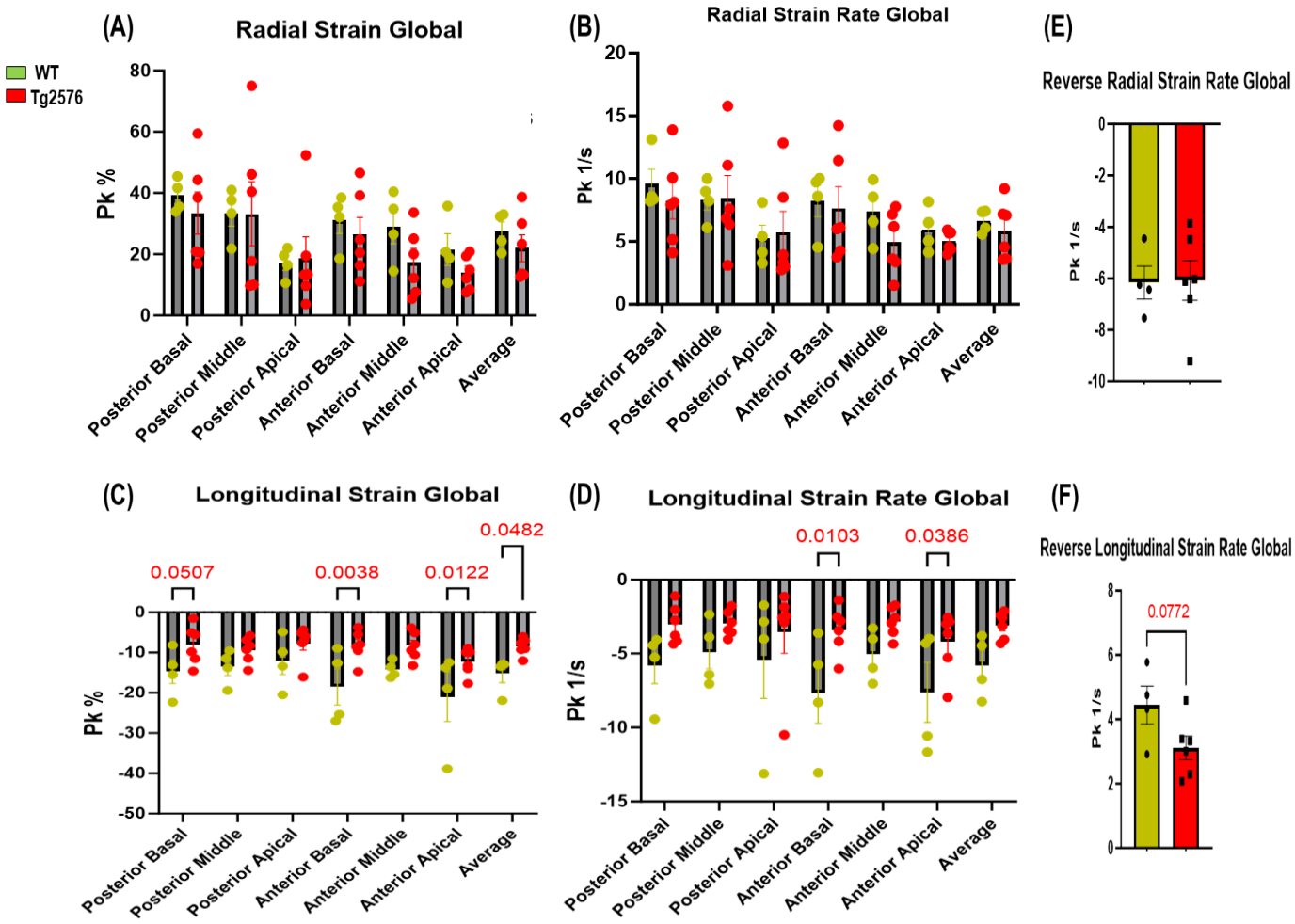

Supplemental Figure 2. Longitudinal strain and strain rate LV contractility are impaired in Tg2576 AD mice. Radial and longitudinal strain or strain rate measured at six LV segments as well as their average (**A-D**), and reverse (diastolic) radial (**E**) and longitudinal (**F**) SR global in 13 months old WT and Tg2576 mice were evaluated using speckle-tracking-based strain echocardiography. Data are presented as a mean±SEM. *P<0.05 and vs WT. n=4-6 mice/group. Two-way ANOVA with Tukey's multiple comparisons post hoc test (**A-D**), and student t-tests (**E-F**) have been performed between the groups.

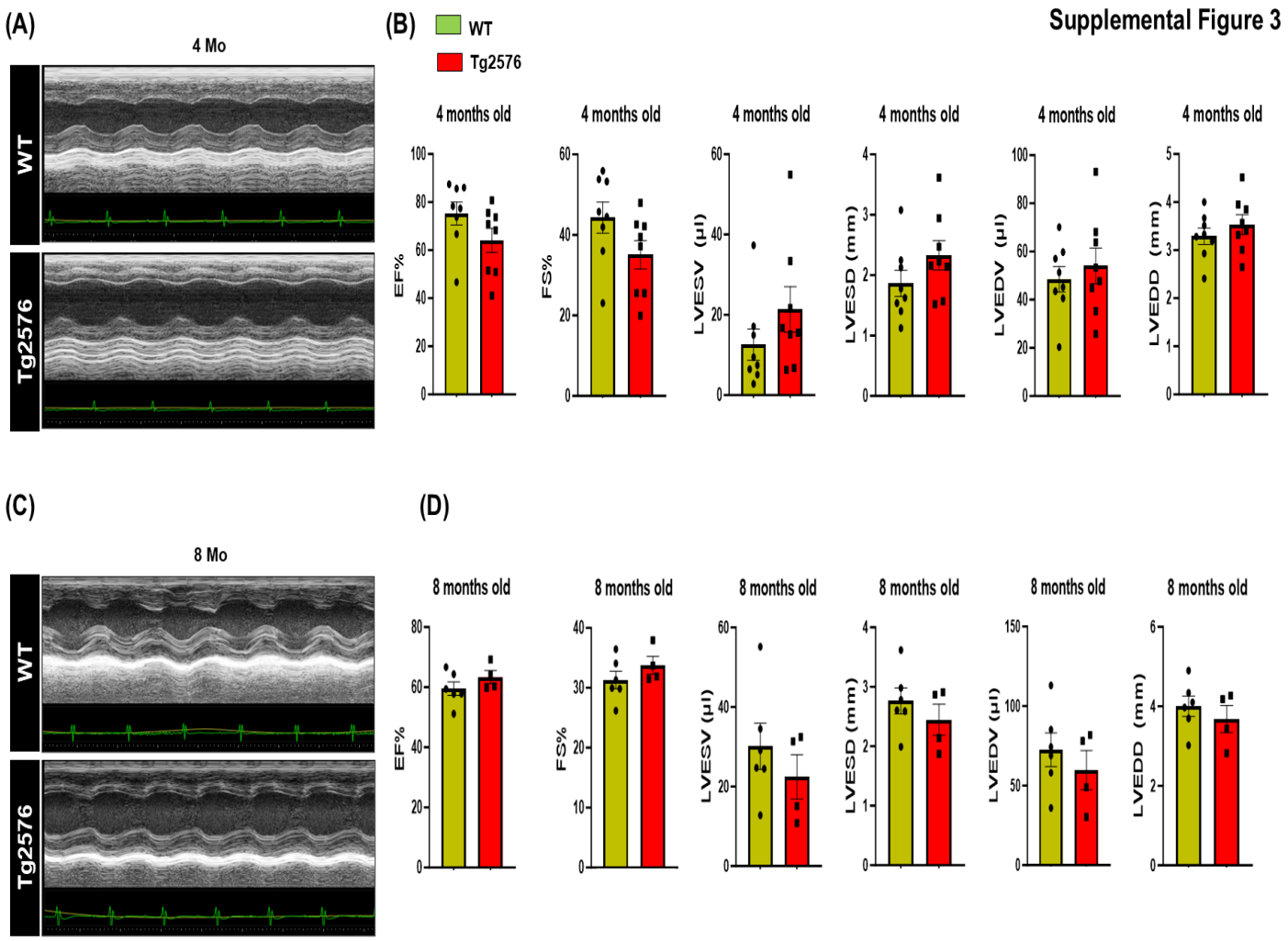

Supplemental Figure 3. Cardiac function is not affected in 4 or 8 months old Tg2576 mice. (**A-C**) Representative M-mode echocardiography images of WT and Tg2576 mice show no difference between the experimental groups. (**B-D**) Ejection fraction (EF%) and fractional shortening (FS%) percentage, left ventricular end-systolic and diastolic diameters (LVESD, LVEDD), and left ventricular end-systolic and diastolic volumes (LVESV, LVEDV) of age-matched (4 and 8-month-old) Tg2576 mice and WT littermates. n=4- 8 mice/group. Data are presented as a mean±SEM. *P<0.05 and vs WT. Student t-tests have been performed between the groups.

Supplemental Figure 4

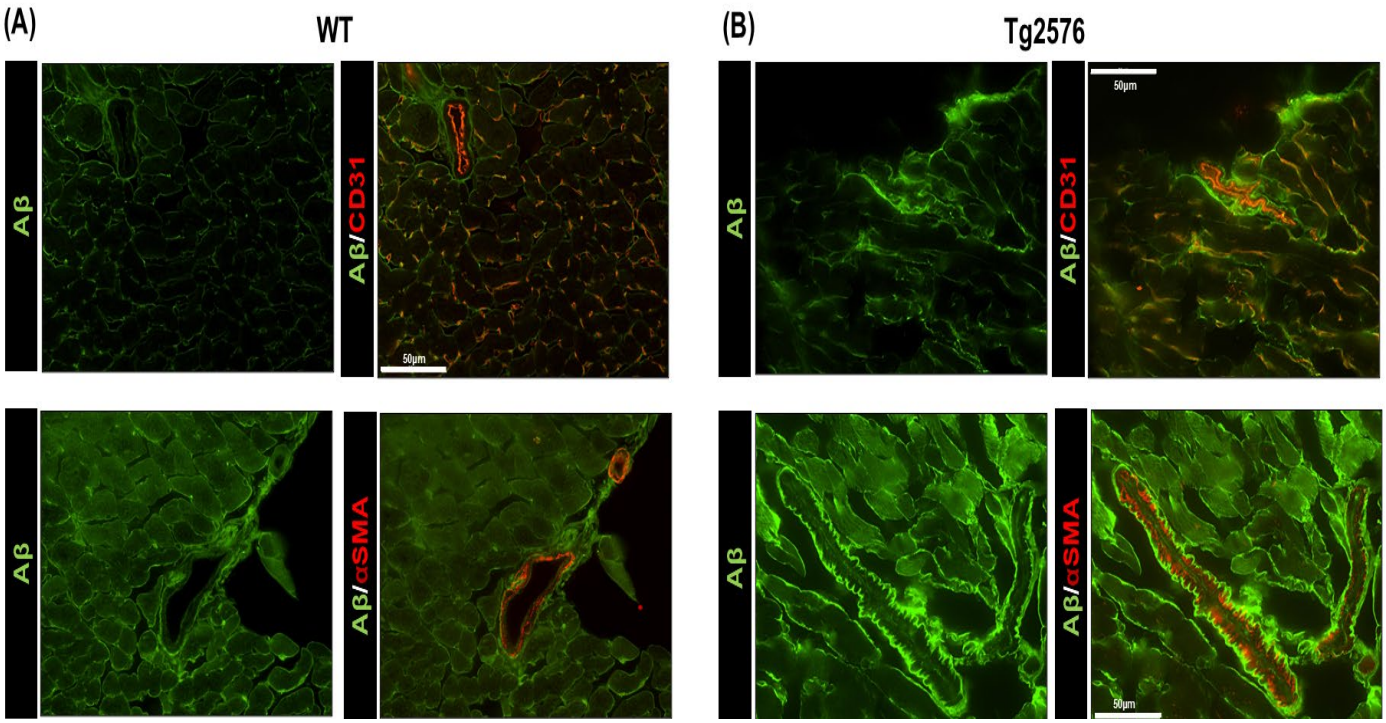

1105

1106 **Supplemental Figure 4. Amyloid-β surrounds cardiac vessels and infiltrates the**
1107 **vascular basal lamina.** (**A**-**B**) Representative digital images (upper panels, scale bar
1108 50μm) showing vessels (endothelial cells stained with CD31, in red) and Aβ (in green),
1109 and representative digital images (lower panels; scale bar 50μm) showing α-smooth
1110 muscle actin (αSMA, staining vascular smooth muscle cells, in red) and Aβ (in green)
1111 in cardiac sections from 13 months old WT and Tg2576 mice.

1112

1113

1114

1115

1116

1117

1118

1119

Supplemental Figure 5

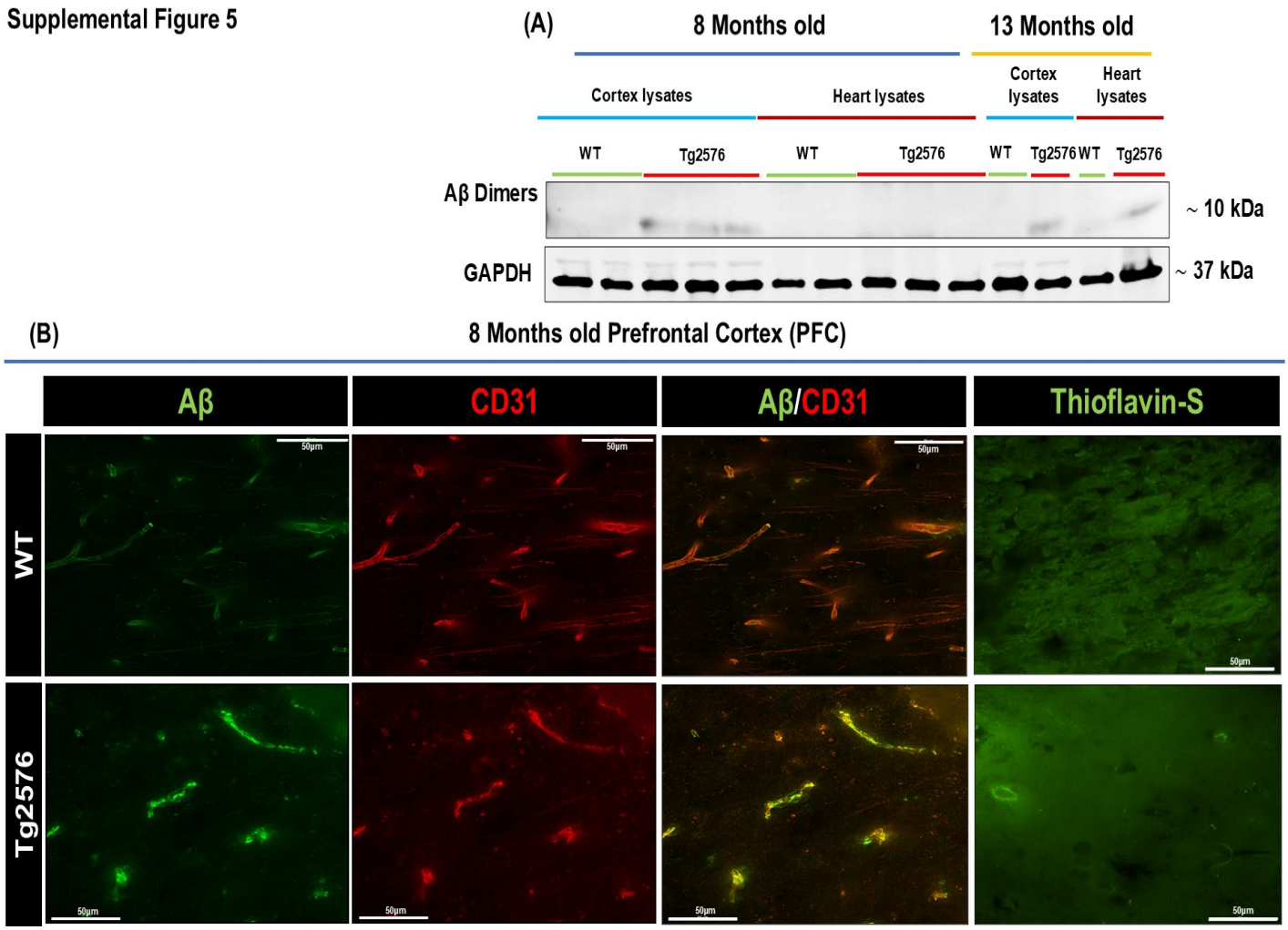

Supplemental Figure 5. Amyloid-β deposits in vessels of 8 months-old Tg2576 prefrontal cortex (PFC), but not in heart tissue. (**A**) Representative immunoblots show Aβ dimers in total cardiac lysates from WT and Tg2576 mice. Tg2576 cerebral cortex lysate was used as an internal positive control. GAPDH levels were used as a loading control. (**B**) Representative digital images (scale bar 50μm) showing vessels (stained with CD31, in red) and Aβ deposits (in green). Right panels: representative digital images (right panels; scale bar 50μm) showing β- sheet conformation (fibrillar) amyloid marked with Thioflavin-S (in green) in the prefrontal cortex (PFC), in 8-months old WT and Tg2576 mice.

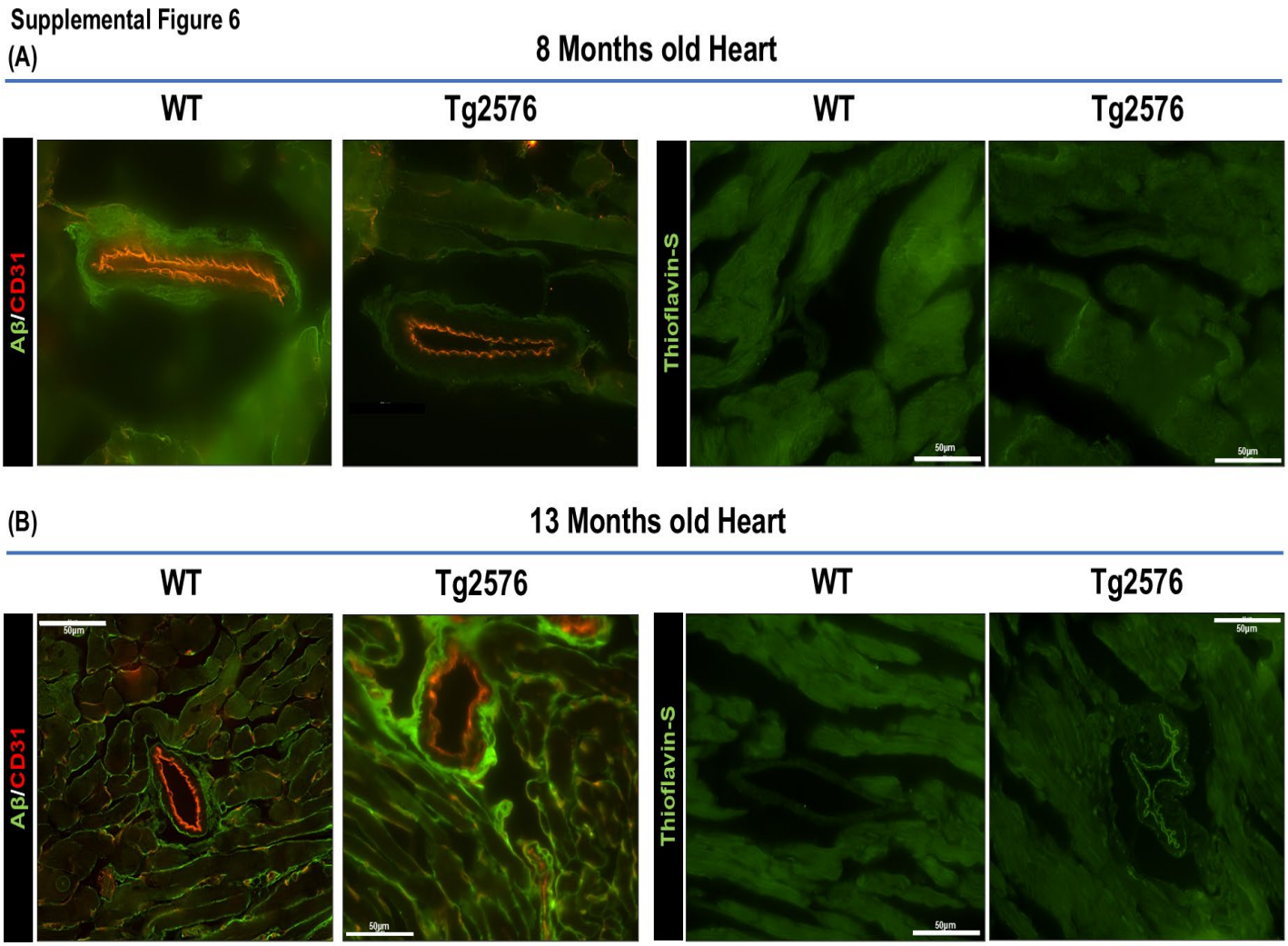

Supplemental Figure 6. AD pathology affects the cardiac vascular network in 13-month-old Tg2576 mice. (**A-B**) Representative digital images (left panels, scale bar 50μm) showing vessels (stained with CD31, in red) and Aβ deposits (in green), and representative digital images (right panels; scale bar 50μm) showing β-sheet conformation of amyloid marked with Thioflavin-S (in green) in cardiac sections from WT and Tg2576 mice.

Supplemental Figure 7

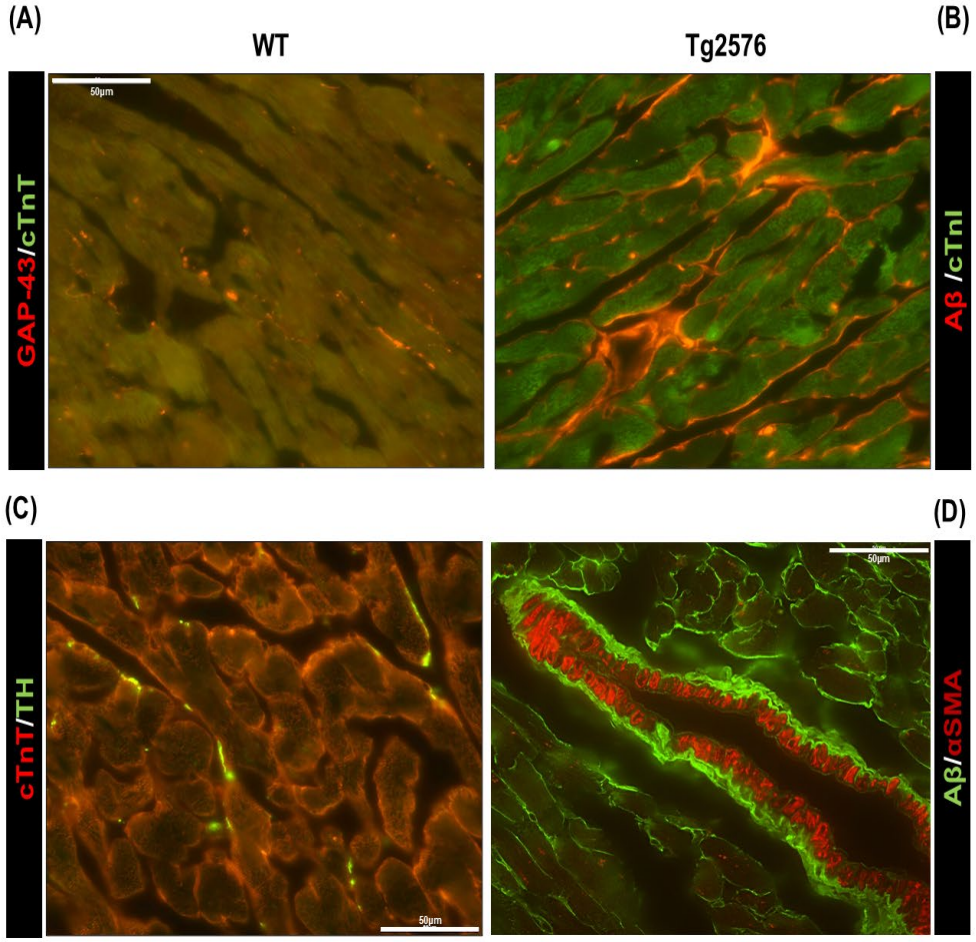

1145

1146 **Supplemental Figure 7.** Representative digital images (scale bar 50μm) of cardiac
1147 sections from 13-month-old WT and Tg2576 mice stained with (**A**) anti-neuronal
1148 regeneration marker (GAP-43, in red) and cardiac Troponin T (cTnT, in green). (**B**) Aβ
1149 (in red) and cardiac Troponin I (cTnI, in green). (**C**) anti-tyrosine-hydroxylase (TH, in
1150 green) and cardiac Troponin T (cTnT, in red). (**D**) Aβ (in green) and α-smooth muscle
1151 actin (α-SMA, in red).

1152

1153

1154

1155

1156

1157

Supplemental Figure 8

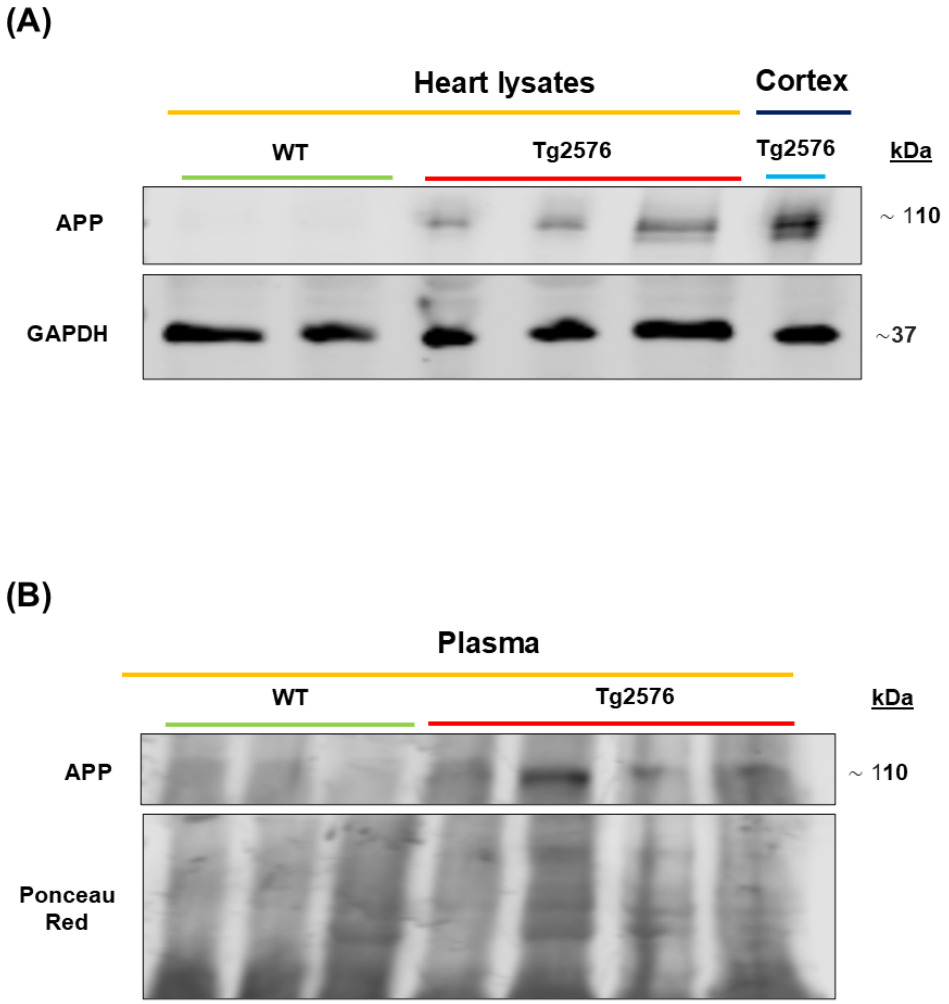

1158

1159 **Supplemental Figure 8. The Amyloid precursor protein (APP) is present in**
1160 **plasma and heart tissue of the 13-month-old Tg2576-AD model.** (**A-B**)
1161 Representative immunoblots showing protein levels of APP in total cardiac lysates
1162 (upper panel) and plasma APP levels (lower panel) in 13-month-old WT and Tg2576
1163 mice. Tg2576 cortex lysate was used as an internal positive control. GAPDH levels or
1164 ponceau red were used as respective loading controls.

1165

1166

1167

1168

1169

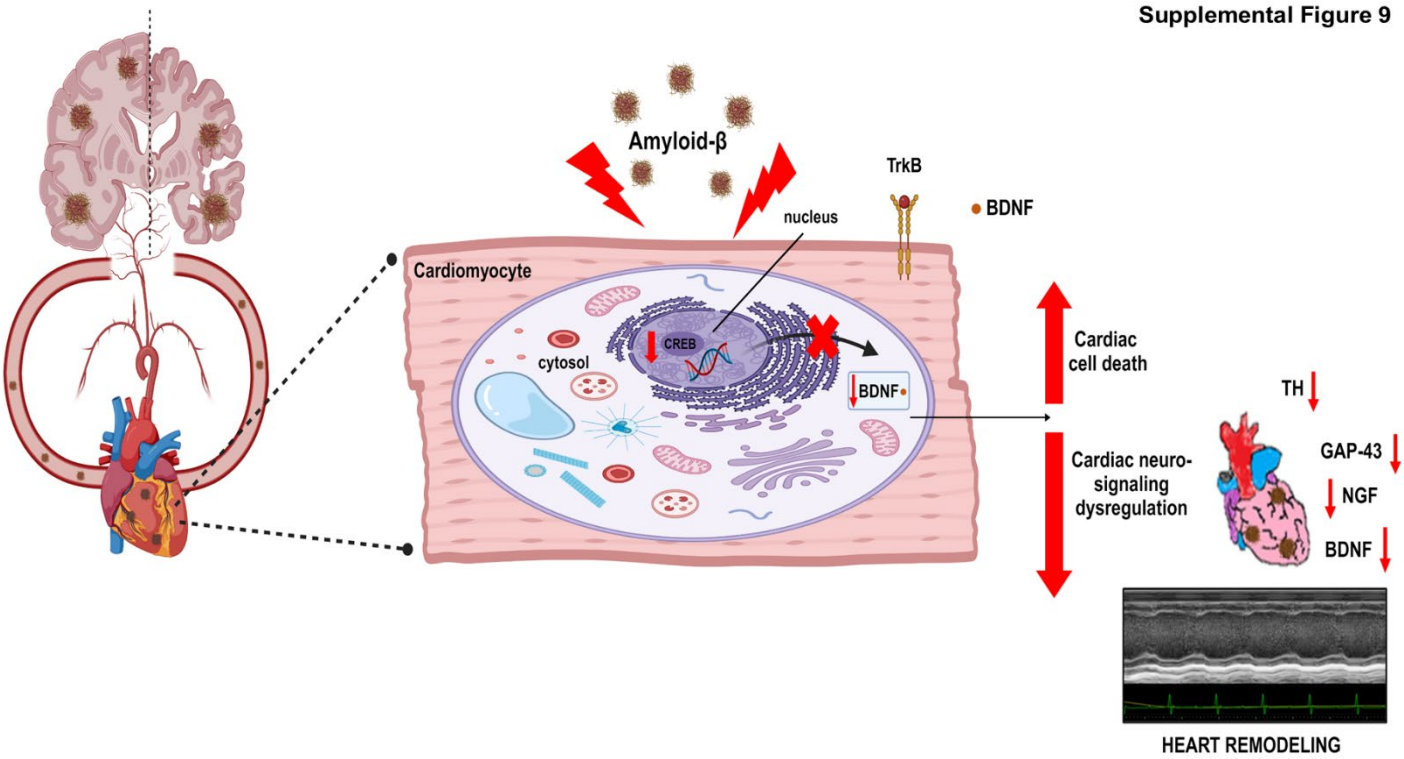

1170

1171 **Supplemental Figure 9. Conceptual scheme of the study**. Amyloid- β aggregates,
1172 present in the heart parenchyma of AD mouse models and AD human hearts, induce
1173 adverse cardiac remodeling and myocardial denervation through cardiac
1174 TrkB/CREB/BDNF neurotrophic signaling axis dysregulation, ultimately resulting in
1175 impaired cardiac physiology.

1176

1177